

## Calculations Pertaining to Hygroscopic Seeding with Flares

WILLIAM A. COOPER AND ROELOF T. BRUINJES

*National Center for Atmospheric Research,\* Boulder, Colorado*

GRAEME K. MATHER

*CloudQuest Ltd., Nelspruit, South Africa*

(Manuscript received 19 April 1996, in final form 13 March 1997)

### ABSTRACT

Some possible effects of hygroscopic seeding with flares are explored by calculating how such seeding would modify the initial size distribution of cloud droplets and the subsequent evolution of that size distribution by coalescence. To be representative of recent experiments in South Africa, the calculations emphasize the effects of hygroscopic particles that can be produced by flares, instead of the larger particles used in most past hygroscopic-seeding experiments. Parcel calculations representing simultaneous condensation and coalescence suggest that the formation of rain through the warm-rain process can be accelerated significantly by the addition of such hygroscopic particles. Some observations of the effects of hygroscopic material near cloud base support at least the early stages of the calculations. The results suggest that the positive effects being obtained in the South African experiment may occur through such acceleration of the warm-rain process. Possible cloud-seeding applications and climate implications are discussed.

### 1. Introduction

Most past hygroscopic-seeding experiments used large salt particles, with diameters of at least 10  $\mu\text{m}$ , to provide embryos for the formation of raindrops. Disadvantages of this approach are that large quantities of salt are needed, dispersion of the salt over areas comparable to a cloud inflow is difficult, and (as emphasized by Klazura and Todd 1978) the growth rates of the particles to raindrops must be matched well to the updraft profile or their growth will be inefficient. Farley and Chen (1975) found that salt seeding only produced a few large drops without significant effect on the precipitation process, unless drop breakup acted to induce a chain reaction that enhanced the effects of seeding. While some positive effects have been attributed to such seeding (e.g., Biswas and Dennis 1971), seeding with hygroscopic material has usually appeared less attractive than seeding with ice nuclei for the preceding practical reasons.

Rokicki and Young (1978) and Tzivion et al. (1994) presented encouraging calculations indicating that the addition of water drops, representing the effect of hygroscopic seeding after a cloud had formed, could have

substantial beneficial effects on precipitation formation in continental clouds. The calculations that follow, however, apply to a different situation, that in which the hygroscopic material is introduced below cloud base. In that case, it can influence the initial condensation process in the cloud, thereby changing the initial droplet size distribution as well as introducing embryos for precipitation growth.

The following calculations simulate simultaneous condensation and coalescence to explore how hygroscopic seeding below cloud base might affect the initiation of coalescence and the production of rain. If the seeding particles are smaller than natural cloud condensation nuclei (CCN), they will not be activated and will have no effect. If they are much larger than natural CCN, they may provide embryos on which raindrops can form. However, for the case where the CCN are comparable to or slightly larger than natural CCN, the consequences are less certain. If the added particles simply modify the natural CCN population to one with similar sizes but higher concentrations, smaller and more numerous droplets would be expected and coalescence would be slower. If the CCN instead are sufficiently larger than natural CCN so that they activate first, they can prevent activation of natural CCN and hence change the character of the initial droplet size distribution, possibly favoring coalescence.

These calculations are motivated by the National Precipitation Research Programme (NPRP) of South Africa, which is using hygroscopic particles produced by air-

---

\*NCAR is sponsored by the National Science Foundation.

---

Corresponding author address: William A. Cooper, NCAR, P.O. Box 3000, Boulder CO 80307-3000.

borne flares to seed summertime clouds. The NPRP approach was developed after Mather (1991) observed apparent enhancement of coalescence in clouds contaminated by particles from a large paper mill. Earlier observations by Hobbs et al. (1970) and Hindman et al. (1977) also suggested a similar connection between paper mills and enhanced precipitation, and there are other reports of precipitation increases downwind of pollution sources (e.g., Schickedanz 1974; Barrett et al. 1979).

There are significant operational advantages to this form of hygroscopic seeding. The amount of salt required is much less, the salt particles are readily produced by flares, and the target area for seeding is an easily identified region at cloud base where the initial droplet spectrum is determined. As with most airborne seeding, a problem facing cloud-base or in-cloud release of seeding material is that diffusion rates are apparently too slow to affect significant parts of a storm during a single ascent (e.g., Weil et al. 1993). For this reason, we focus on mechanisms that might enhance the concentration of drizzle-size droplets (of about 100- $\mu\text{m}$  diameter) because such drizzle mixed throughout a cloud might affect regions much larger than those seeded during a single ascent of a parcel in a strong updraft.

In this paper, calculations of the expected rates of coalescence are used to illustrate the possibility that hygroscopic seeding might accelerate coalescence. The hygroscopic particles are assumed to have the size distribution produced by the flares used in the NPRP, although some other similar size distributions are used to evaluate the relative importance of different parts of the size spectrum. The study emphasizes particles having diameters of 0.5–10  $\mu\text{m}$  because this appears to be the important range of sizes produced by the seeding flares. These particles are much larger than most natural CCN and hence activate first, thus participating in the determination of the droplet size distribution at cloud base. The result can be a broadened droplet size distribution, larger droplets more favorable to coalescence, and sometimes *lower* initial droplet concentrations in the seeded cases.

## 2. Observed size distributions of droplets and of the seeding material

### a. The seeding material produced by flares

The size distribution of particles from the seeding flares used in the NPRP is shown in Fig. 1. The measurements were made using a passive cavity aerosol spectrometer probe (PCASP) and a forward scattering spectrometer probe (FSSP), both manufactured by Particle Measuring Systems, Inc. For these measurements, the instrumented Learjet of South Africa was flown about 50 m behind a seeding aircraft that was burning two of the flares. The Learjet was slowed to the flight speed of the seeding aircraft (about 90  $\text{m s}^{-1}$ ), so air-speed corrections to the FSSP measurements were not

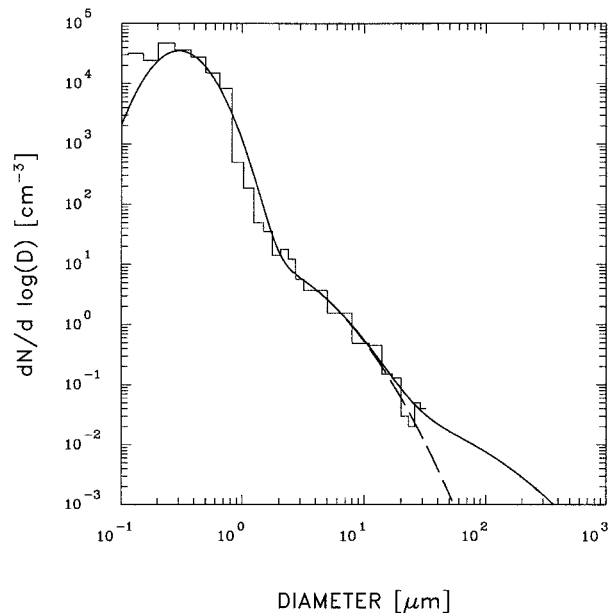


FIG. 1. Size distribution of particles measured at a distance of about 50 m behind the seeding aircraft, during in-trail flight in dry air (with relative humidity of about 30%). The smooth solid curve is the sum of three lognormal distributions, as described in the text; the dashed curve is based on all but the largest lognormal component.

large. The correct index of refraction for potassium chloride (KCl), the primary constituent in the smoke produced by the flares, was used in calibration of the PCASP. However, no corrections to the (water) calibration of the FSSP were applied. For diameters larger than 3  $\mu\text{m}$ , the size distribution may be inaccurate not only because of the possible 10%–15% undersizing that would arise for spheres having the index of refraction of potassium chloride but also because scattering from the faces of irregular particles of (cubic) potassium chloride crystals might invalidate the size calibration of the FSSP for these sizes.

An extension of the size distribution to diameters larger than 40  $\mu\text{m}$  is included in Fig. 1. The extrapolation is based on measurements from a PMS 2D spectrometer, not shown, from a different set of flights. The upper curve in Fig. 1 will be taken here to represent an upper limit because such particles might still have been burning at the location where they were observed or might be aggregates having mass much smaller than represented by their measured size. It was possible to see still-burning fragments pass the aircraft during in-trail measurements of the seeding material, so the largest particles are probably not present in the final product from the flares. The lower distribution shown by the dashed line will be used in all calculations except some to investigate the possible effects of very large particles.

As shown in Fig. 1, the measured size distribution from the flares can be approximated by the sum of two or three lognormal distributions. As used here, the three distributions have respective geometric mean diameters

of 0.3, 1.0, and 10  $\mu\text{m}$ , and geometric standard deviations (relative to base-10 logarithms) of 0.2, 0.4, and 0.6. The dashed curve in Fig. 1 is the sum of the first two lognormal distributions, and the solid curve is the sum of all three. The ratios of concentrations used for the three lognormal distributions were  $1:1.7 \times 10^{-4}:3 \times 10^{-7}$ . The second distribution adds most of the particles having diameters from 2 to 20  $\mu\text{m}$  in the figure, and the third those larger than about 30  $\mu\text{m}$ . By representing the distribution in this way in the calculations that follow, it is convenient to vary the relative concentrations of these different parts of the size distribution and thus determine which are more influential in the effects that result.

### b. Observed size distributions of cloud droplets

Some measurements of the sizes of cloud droplets in seeded clouds help illustrate the effects that hygroscopic seeding may have near cloud base. The instrumented Learjet of South Africa, in conjunction with a separate seeding aircraft, was also used for these measurements. The high speed of the aircraft introduces some uncertainty into measurements of sizes from the FSSP, so emphasis was placed on obtaining nearby measurements of droplet sizes within and outside of seeding plumes while similar flight conditions were maintained. The Learjet initially flew in trail behind the seeding aircraft until a good updraft was identified and the plume was observed rising into the cloud base. Then the Learjet climbed into the cloud base and flew at right angles across the line of seeding in order to intercept the rising plume.

Figure 2 shows an example of an unusual change in the droplet size distribution observed during one such climb. The two droplet size distributions were collected at the same altitude above cloud base, and they contain approximately the same liquid water content (0.33 vs 0.35  $\text{g m}^{-3}$ ). Both values are near the value of 0.38  $\text{g m}^{-3}$  expected for unmixed ascent from the cloud base, observed to be 200 m below this level. There was a substantial decrease in total concentration (280 vs 508  $\text{cm}^{-3}$ ) and a corresponding increase in the sizes of the largest droplets for the sample thought to be in the seeding plume. These observations suggest that the seeding material may increase the concentrations of large droplets and broaden the droplet size distribution. They also suggest the unexpected possibility that seeding may decrease the total concentration of droplets in the cloud.

## 3. The numerical approach

### a. General features

The calculations used in this paper represent the effects of condensation and coalescence during adiabatic ascent of a closed parcel. In such a calculation, reassignment of droplets to categories or "bins" during the

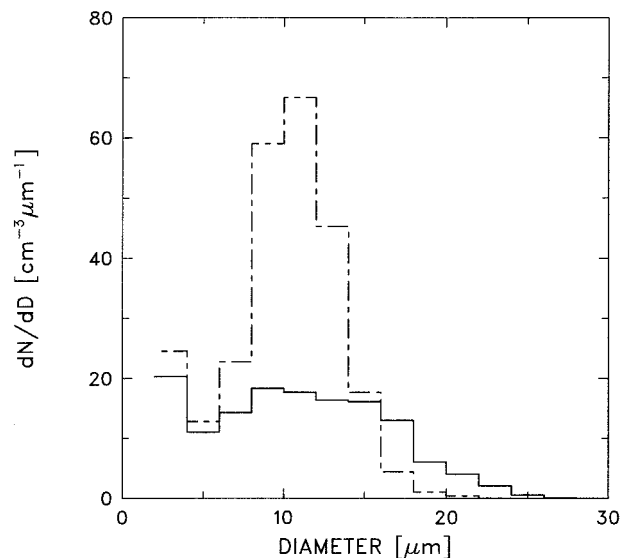


FIG. 2. Droplet size distributions measured about 200 m above cloud base in a seeded cloud. The dashed curve shows an example of the typical size distribution observed in most of the cloud and thought to be natural, while the solid distribution is one observed at the expected location of the plume and thought to be the result of seeding. (Observations from 19 December 1992, 1412:42 and 1412:54, pressure 746 mb and temperature 13.3°C.)

calculation can lead to artificial broadening of the droplet size distribution, so growth by condensation was treated by allowing the size assigned to each bin to change without any reassignment of droplets to new bins. This avoids the need for interpolation among the bins and so permits very accurate calculation of the initial size distribution. Indeed, the droplet sizes tend to grow closer together during condensation, so this approach uses variable bin locations in a way that concentrates the bins where resolution is needed.

The disadvantage of using variable bins is that these are not compatible with the Berry and Reinhardt (1974a, b) approach to coalescence unless interpolation is used, and such interpolation eliminates the advantage of using variable bin sizes. For this reason, a modified Kovetz and Olund (1969) scheme was used. Although their scheme is compatible with variable bin sizes, it is known that it produces erroneously fast growth of the largest drops (e.g., Scott and Levin 1975). To reduce this error, a modification (discussed later) was introduced that reduced this bias and produced improved agreement with test cases.

To represent the effects of simultaneous condensation and coalescence, the diameters of all particles in a particular bin were increased as required by condensation, while droplets were reassigned among the bins to represent coalescence. This has several other advantages not evident in the current application. For example, the solute content in the droplets can be traced easily during condensation, and other algorithms for coalescence (e.g., Gillespie 1975) can be incorporated conveniently.

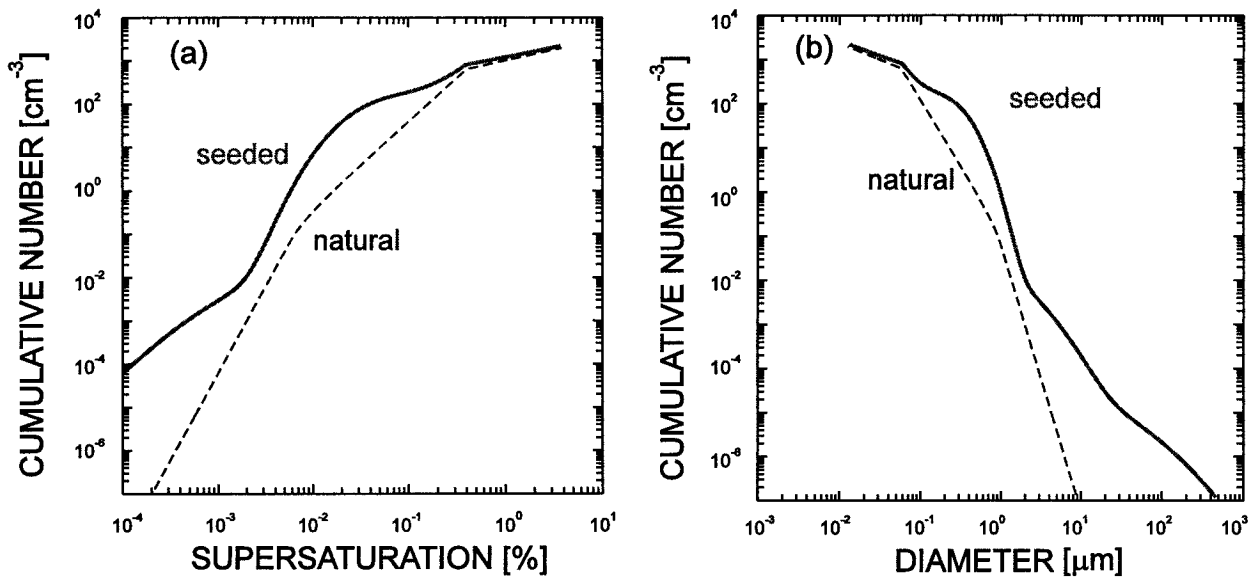


FIG. 3. (a) Cumulative concentration of CCN as a function of supersaturation for natural and seeded cases representing continental conditions. The corresponding size distribution is shown in Fig. 3b. (b) Cumulative size distribution of soluble particles (ammonium sulfate) corresponding to the CCN activity distributions of Fig. 3a.

### b. Activation of droplets and growth by condensation

#### 1) REPRESENTATION OF THE CCN SPECTRUM

Several different choices for the CCN activity distributions as functions of supersaturation are used in this paper. For the central plains of South Africa, some measured distributions could be represented approximately by the values  $C_1 = 1000 \text{ cm}^{-3}$  and  $k = 0.5$  in the formula

$$N(S) = C_1(S/S_0)^k, \quad (1)$$

where  $N(S)$  is the cumulative number of CCN active at or below the supersaturation  $S$ , and  $S_0$  is the reference supersaturation (conventionally 1%) at which the cumulative concentration equals  $C_1$ . In this paper these values of  $C_1$  and  $k$  will be used to represent continental clouds. For a maritime extreme, the values  $C_1 = 50 \text{ cm}^{-3}$  and  $k = 0.7$  [as measured near Hawaii by Hudson (1993; J. Hudson 1991, personal communication)] will be used. In addition, an intermediate CCN population with  $C_1 = 300 \text{ cm}^{-3}$  and  $k = 0.7$  will be considered. The CCN concentrations measured by Hobbs et al. (1985b) to be representative of the lower troposphere over the High Plains of the United States fall between the intermediate and continental cases.

The assumed CCN distribution (1) must be modified for the largest particles because otherwise for soluble particles (1) gives a total CCN mass that is infinite for any  $k < 2$ . Measurements by Alofs and Liu (1981) suggest that there is a change in slope at a supersaturation of about 0.05%; they report that the slope parameter  $k$  is about 3.85 for supersaturations lower than this. However, there is also extensive evidence for a prevalent "Junge" distribution of particles with sizes of about 0.1–1.0 μm, which for soluble particles would require

a slope parameter of  $k = 2.0$ . Therefore, the natural CCN size distributions used in this paper include three regions to give the form in (1) at the smallest sizes, a Junge distribution at intermediate sizes, and a still faster decrease in concentration with radius at the largest sizes. For the intermediate (Junge) region, with supersaturations from 0.007% to 0.4%, the distribution was characterized by

$$\frac{dF(r_a)}{d \log r_a} = \frac{A}{r_a^3}, \quad (2)$$

where  $F(r_a)$  is the cumulative number of CCN with radius exceeding  $r_a$  and  $A$  was chosen to be  $10^{-13}$  for the continental cases and  $10^{-14}$  for the maritime cases. For still lower supersaturations, (2) was changed to have a slope parameter of  $k = 4.0$  for diameters above 1 μm, to be consistent with the Alofs and Liu (1981) data, or  $k = 6.0$  to represent an extreme case with very few giant particles. The concentration for these sizes was selected to give a continuous match to the intermediate size range.

Two CCN distributions to be used for seeded and unseeded cases are shown in Figs. 3a and 3b. While some natural giant particles were included, the total concentration with diameters larger than 10 μm was only about  $0.1 \text{ m}^{-3}$ . This is much smaller than the concentration of such particles used by Johnson (1982), for example, or found to be representative of the continental boundary layer in the observations of Hobbs et al. (1985a). Although the distribution in Fig. 3 underestimates the concentration of particles in the 10–100-μm range, all particles are assumed soluble, so some adjustment to the measured size distributions of (mostly

insoluble) particles is needed. Some evaluation of the effects of higher background concentrations of giant particles is included in a later section.

The seeding material was assumed to have the size distribution shown in Fig. 1, except that the measured concentration was reduced by a factor of 100 to allow for dilution before this plume entered cloud base. The particles were assumed to be potassium chloride, the primary constituent produced by the flares.

## 2) ACTIVATION OF CCN

In these calculations, the early development of haze droplets below cloud base was not calculated. Instead, CCN activation was treated by introducing new drops into the calculations at a size that would be in equilibrium at 95% relative humidity. This choice, made to provide some partial representation of the lag that would characterize growth of the largest CCN, was a compromise that had little effect on the growth of typical small CCN. At water saturation, hygroscopic particles having diameters smaller than about 10  $\mu\text{m}$  deliquesce to form solution droplets in less than 1 s, while particles having diameters of about 100  $\mu\text{m}$  deliquesce in a few minutes, so most of the haze droplets would be near equilibrium with the ambient humidity. However, hygroscopic particles having diameters of about 1 mm would take several hours to deliquesce by diffusion, and their growth as haze droplets would lag far behind the equilibrium size for the ambient relative humidity in the updrafts assumed for these calculations. If they were introduced at equilibrium sizes corresponding to 100% relative humidity, they would be unrealistically large and would have an exaggerated influence on the development of coalescence.

When the calculation started, all droplets were assigned to logarithmically spaced bins so that the ratio of the masses or radii of adjacent bins was constant. Typically, 256 bins ranging from 0.01  $\mu\text{m}$  to 1 cm were used, so that each decade in the logarithmic representation of radius was divided into about 43 bins.

## 3) REPRESENTATION OF DIFFUSIONAL GROWTH

Once activated, droplets were assumed to grow in accord with the Fukuta and Walter (1970) representation of the droplet growth equation, with an assumed condensation coefficient of 0.04 and an accommodation coefficient of 1.0. The mass of solute in the original CCN was used at each step to calculate the growth rate because (especially for the seeded CCN) this mass was large enough to influence the growth rate while the supersaturation maximum was approached near cloud base. Natural and seeded CCN were taken to be ammonium sulfate and potassium chloride, respectively.

Because the growth rate during condensation or evaporation is approximately linear in time if represented in terms of the square of the radius  $r$ , finite-difference

changes were applied to  $r^2$  rather than to  $r$ . Growth by condensation was represented by increasing the mass assigned to each bin, so all droplets in each bin grew at the same rate. The size-dependent influences of dissolved solute and surface tension, known to be important in determining the initial breadth of the droplet size distribution, were retained in the calculations. The growth calculation also included the effects of solute concentration on the surface tension, the activity coefficient, and the density of the solution. However, the largest uncertainties arose from the choice of condensation coefficient and accommodation coefficient. The formulas used are given in appendix B.

## 4) TRACKING THE SUPERSATURATION

Water vapor pressure was used as the prognostic variable, and temperature was diagnosed using the assumption that ascent was adiabatic. Specifically, the interaction between supersaturation and temperature was incorporated by calculating the wet-equivalent potential temperature (cf., e.g., Paluch 1979) at cloud base, then using the conservation of this quantity and of the total mixing ratio during adiabatic processes to calculate subsequent temperatures from the vapor pressure. At each time step, the vapor pressure was decreased by the calculated condensation rate<sup>1</sup> and then in proportion to the pressure change. The resulting water-vapor mixing ratio was used at the new pressure to find the temperature giving the cloud base value of the wet-equivalent potential temperature, and this temperature was used to calculate a new value of the saturation ratio.

The method used to select the time step is described in appendix B. Because the integration scheme used a variable time step, to guard against instability the time step  $\Delta t$  was constrained to satisfy

$$\Delta t \leq 0.5 \tau_{qs} \frac{S_{\max}}{S}$$

after the initial activation region at cloud base. In this formula,  $\tau_{qs}$  is the relaxation time constant for the water vapor field [cf., e.g., Cooper (1989) for the expression used for this time constant] and  $S_{\max}$  is the maximum supersaturation reached during activation of the droplet spectrum near cloud base. This approach permitted accurate tracking of the supersaturation even in those cases where accelerating parcel ascent or significant depletion of the cloud droplets caused renewed CCN activation.

## c. Coalescence

To be compatible with the variable bin sizes used to represent condensation, a modified Kovetz and Olund

<sup>1</sup> Because the total-water mixing ratio remains constant, the derivative  $d\epsilon/d\chi$  is  $-RT/(M_w + r_i M_a)$ , where  $r_i$  is the total-water mixing ratio determined from the water vapor mixing ratio at cloud base, and other symbols are as in appendix A.

(1969) scheme was used. The Kovetz–Olund algorithm assigns drops resulting from collisions to the two bins bracketing the correct size, in proportions chosen to conserve mass in the collision. This leads to some acceleration of the growth of the largest drops, as demonstrated by Scott and Levin (1975), because the interpolation distributes the resulting mass between two adjacent bins and so leads to numerical broadening of the size distribution.

To try to improve upon the performance of the Kovetz–Olund algorithm for the growth of the largest drops, the following modification was introduced. Instead of interpolating between the bins bracketing the correct size of the drop resulting from a collision, drops were assigned to the bin nearest to the correct size, but the average size assigned to that bin was then modified to conserve mass. The advantage of this modification is better representation of large drops growing at the expense of small cloud droplets. In the Kovetz and Olund scheme, such drops can grow only in discrete jumps, by increasing the number assigned to the next larger bin, so some drops reach the next bin with each time step even if the real situation is that it takes many time steps for any drops to increase in mass by a full bin. In the scheme used here, such collection is represented by slowly increasing the mass assigned to the bin of the collector drops. Because the growth of large drops is mostly via collisions with cloud droplets until the cloud droplet population is depleted, accurate representation of these collisions is an advantage of the modification introduced here.

The primary disadvantage of this modified scheme is that, when a collision produces a drop that doesn't match the size of any bin, adjustment of the sizes of all other drops in the nearest bin is required to conserve mass while preserving a unique mass assignment for the bin. This sometimes causes bins to grow far apart or very close together. For the calculations reported in this paper, new bins were introduced whenever the bin spacing grew to twice the initial spacing, so that artificial gaps would not result from the lack of nearby bins to which to assign drops. Also, to avoid excessive growth in the number of bins and unnecessarily slow calculations, bins were averaged together whenever they were spaced more closely than one-fourth the initial spacing.

This scheme was tested against the analytical results of Golovin (1963) and Scott (1968), and successfully reproduced those results with practical time steps and bin sizes, as shown in appendix C. The errors were in the direction of *underestimating* the growth at largest sizes, but a series of tests all showed predictions that were consistent with the analytical solutions to a few percent. (An underestimate is expected because the most likely result of a collision is a mass that is smaller than the mass assigned to the nearest logarithmically spaced bin, when the masses are increasing from initially small values.) The results were significantly improved over the unmodified Kovetz and Olund scheme, which was

also tested for these calculations. Appendix C also shows that the results were in good agreement with corresponding calculations, for coalescence only, using the method of Berry and Rinehardt (1974a, b).

The collision efficiencies were taken to be those of Klett and Davis (1973). For radii larger than 70  $\mu\text{m}$ , the Beard and Grover (1974) representations of the collision efficiencies were used. Coalescence efficiencies as parameterized by Beard and Ochs (1984) and used in similar calculations by Ochs and Beard (1985) were included in these calculations, but the detailed size distributions resulting from breakup were not; instead, collisions not resulting in coalescence were assumed to preserve the initial drop sizes. Because, in the course of initial precipitation development, most collisions are between growing collector droplets and cloud droplets, this approximation should be adequate, and it avoids the lengthy parameterization of the Low and List (1982) representation of breakup. To avoid unrealistically large drops, the concentrations of drops larger than 6 mm in diameter were assumed to decrease with an exponential time constant of 10 s, and the mass from such drops was reinserted at the 6-mm size. This avoided rapid growth of the small concentration of such drops, which otherwise might produce unrealistic depletion of the liquid water content. The absence of a 6-mm spike in the final distributions presented in this paper is evidence that the assumed breakup process did not influence the final distributions.

A significant deficiency in the approach taken here is that sedimentation is not included (except to the extent that the collision kernel depends on the different fall speeds of the colliding drops). This leads to quite unrealistic results by the time the calculation ends because millimeter-size drops have formed that have fall speeds comparable to the assumed updrafts. This same weakness applies to many other standard coalescence calculations, and these results can be compared to that earlier work. Because the objective is to determine if the warm-rain process can be accelerated by hygroscopic seeding, we rely only on qualitative conclusions from these calculations; the quantitative results require considerable interpretation to compensate for this and other weaknesses of the closed parcel model.

Additional details regarding the numerical integration scheme are presented in appendix B. Typical integrations used time steps of 0.1 s or smaller near cloud base, and 1–10 s (depending on updraft profile) once the parcel rose more than 100 m above cloud base. Mass conservation was enforced by the selected calculation scheme, so changes in total water substance could result only from numerical rounding. Water substance was normally conserved to better than  $1 \times 10^{-5}$  relative error.

#### 4. Calculations to illustrate seeding effects

##### a. Sounding and CCN distributions

Some special calculations, constructed to illustrate possible seeding effects rather than to represent realistic

clouds, are presented in this section. A temperature sounding from South Africa (shown in detail later, as Fig. 6) was used for levels below 550 mb, but above 550 mb the sounding was modified by the introduction of an artificial stable ( $+30^{\circ}\text{C}$ ) layer to inhibit any further ascent. Cloud base pressure was 700 mb where the temperature was  $+13^{\circ}\text{C}$ . In this sounding, a parcel was allowed to rise as driven by buoyancy from cloud base (with an initial cloud base updraft of  $3\text{ m s}^{-1}$ ) until the parcel again reached zero vertical velocity about 1700 m above cloud base and about 3 min after passage through cloud base. The liquid water content at that altitude was about  $2.5\text{ g m}^{-3}$ , but the high assumed CCN concentration led to the activation of a droplet concentration of  $994\text{ cm}^{-3}$ , and mean droplet radii were only about  $9\text{ }\mu\text{m}$  at the top of this ascent. Even though the parcel was negatively buoyant at the level when it stopped rising, the parcel was then arbitrarily held at this level to provide a total growth time of 30 min after passage through cloud base.

In these calculations, "unseeded" conditions were represented by the natural CCN spectrum of Fig. 3, except that, to suppress possible effects of giant CCN, the slope of the size distribution for CCN with diameters larger than about  $1\text{ }\mu\text{m}$  was assumed to decrease in proportion to  $r^{-9}$ , where  $r$  is the particle radius, instead of  $r^{-6}$  used for Fig. 3 and for later calculations in this paper. This corresponds to a slope parameter for the CCN distribution of  $k = 6$  instead of  $k = 4$  for the largest particles. To represent the effect of seeding, hygroscopic particles having various sizes and concentrations were added to this CCN spectrum.

#### b. The unseeded case

Figure 4a shows the calculated droplet size distributions, near cloud base and after 10, 20, and 30 min of growth, for the unseeded CCN spectrum. After 20 min, less than  $10^{-6}\%$  of the condensate was converted to precipitation (taken here to be condensate in drops with diameters larger than  $0.5\text{ mm}$ ), the concentration of such drops was still less than  $0.0001\text{ m}^{-3}$ , and the drizzle concentration (with diameters greater than  $100\text{ }\mu\text{m}$ ) was less than  $0.1\text{ L}^{-1}$ . Even after 30 min, only 0.02% of the condensate was converted to raindrops, and the raindrop concentration was still smaller than  $3\text{ m}^{-3}$  although the concentration of drizzle drops had exceeded  $1\text{ L}^{-1}$ . Thus, no significant initiation of the coalescence process occurred in 30 min.

#### c. Effects of the seeding material from the flares

Figure 4b shows the result when the preceding conditions are modified by the addition of seeding material, in a concentration of  $150\text{ cm}^{-3}$  and with the size distributions shown in Fig. 1. The initial cloud base size distribution in the seeded case was slightly broader and extended to significantly larger sizes than in the un-

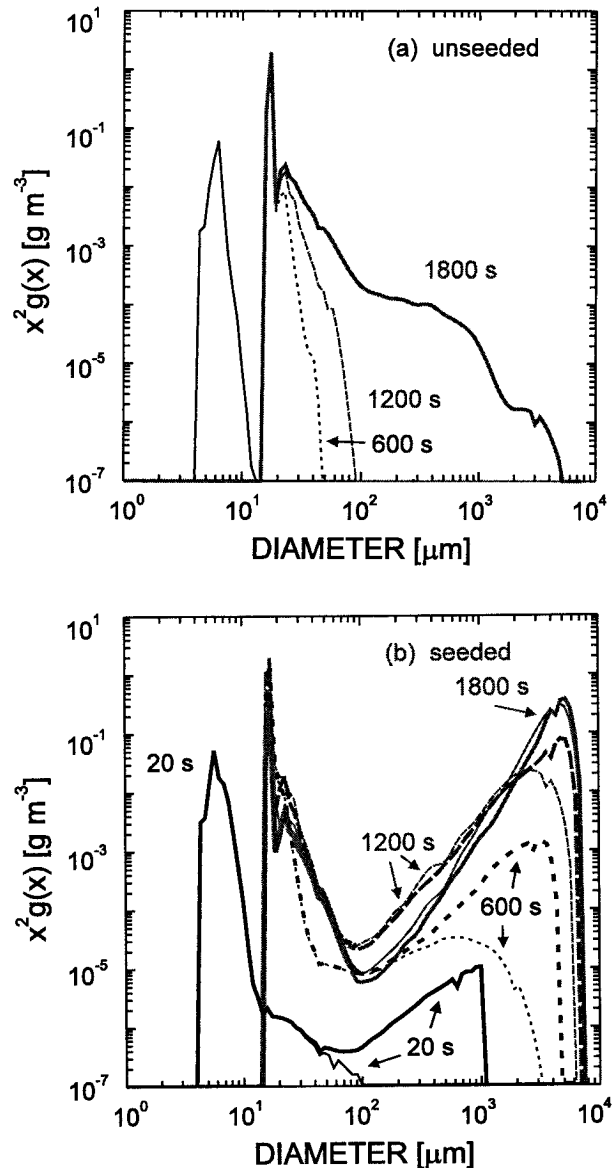


FIG. 4. (a) The mass distribution functions 20, 600 (dotted line), 1200 (dashed line), and 1800 s after passage through cloud base for the unseeded case. The distribution function  $g(x)$  (where  $x$  is the cloud droplet mass) is weighted by  $x^2$  to show the distribution of liquid water content with the logarithm of mass. The true abscissa for this distribution function is mass  $x$ , but the abscissa is labeled here in terms of equivalent droplet diameter. The ordinate in these plots is equal to one-third of the distribution function  $g(\ln r)$  used by Berry and Rinehardt (1974a, b) to display the liquid water content. (b) Mass distribution functions, as in Fig. 4a, for the seeded case. The two curves shown for each time represent the two different size distributions shown in Fig. 1, the thin lines excluding the largest particles and the thick lines including those particles.

seeded case. Drizzle droplets appeared in concentrations exceeding  $80\text{ m}^{-3}$  after only 10 min. After 20 min, the calculations that included the largest particles converted about 25% of the condensate to raindrop sizes, the drizzle concentration was  $0.4\text{ L}^{-1}$ , and the raindrop con-

centration grew to more than  $100 \text{ m}^{-3}$ . After 30 min, 85% of the condensate was converted to precipitation.

When the largest particles were excluded, the calculated development of rain was slower in the early stages but almost the same as for the full size distribution after 20–30 min. It took 22 min instead of 20 min to reach 25% conversion to precipitation, and after 30 min 82% instead of 85% of the condensate was converted to precipitation. The final raindrop size distributions and the intermediate distributions were also quite similar. This result suggests that the largest particles, even if present, would not be responsible for most of the precipitation that forms after 20–30 min, but might produce trace amounts of early precipitation. Because these largest particles are probably not present in the final product from the flares, they will not be included in subsequent calculations in this paper.

#### d. Effects of the smallest particles from the flares

To determine the effects of the smallest particles in the flares, these calculations were repeated for seeding only with the size distribution given by a lognormal distribution having a geometric mean diameter of  $0.3 \mu\text{m}$  and a geometric standard deviation of 0.2, as was used to represent the main part of the distribution in Fig. 1. The result was that, for a total seeding concentration of  $150 \text{ cm}^{-3}$ , precipitation development was slightly slower than for the control case. It thus appears that the high concentration of small particles produced by the flares is not beneficial because it is too similar in size to natural CCN. Instead, the intermediate portion of the size distribution of Fig. 1, represented by a geometric mean diameter of  $1 \mu\text{m}$  and geometric standard deviation of 0.4, was primarily responsible for the enhanced rate of precipitation formation. Indeed, repeating the calculations with only this  $1\text{-}\mu\text{m}$  component gave results essentially the same as those obtained when the smaller particles were also included.

#### e. Using $1\text{-}\mu\text{m}$ particles

To consider the possible effects of a narrow distribution of  $1\text{-}\mu\text{m}$  particles, the calculations were repeated for seeding with  $150 \text{ cm}^{-3}$  particles with a geometric mean diameter of  $1 \mu\text{m}$  and a smaller geometric standard deviation of 0.2. The results for this case are shown in Fig. 5. The initial size distribution was significantly broader than in the control case and developed pronounced bimodality. When the cloud droplets grew to a mean diameter of about  $10 \mu\text{m}$ , the coefficient of variation (or dispersion) of the droplet size distribution was 0.17, while in the control case it was only 0.04. Although after 20 min only 1% of the condensate was converted to precipitation in this case, a high concentration of drizzle drops ( $25 \text{ L}^{-1}$ ) had formed, and these drizzle droplets then produced a rapidly accelerating

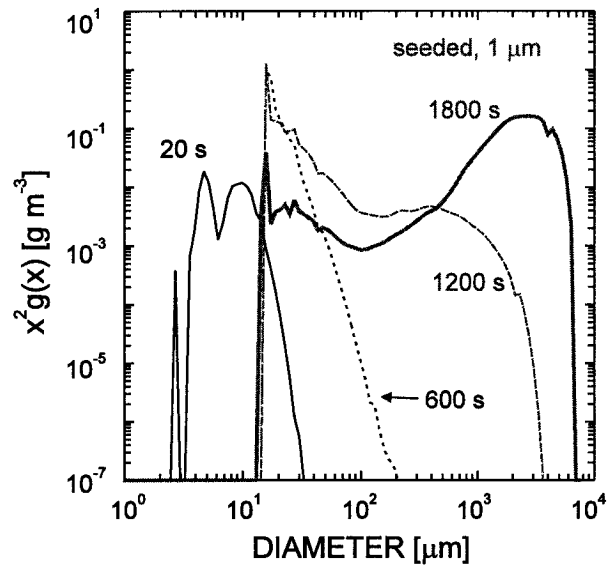


FIG. 5. Mass distribution functions, as in Fig. 4, for seeding with  $150 \text{ cm}^{-3}$  potassium chloride particles having a size distribution with geometric mean diameter of  $1 \mu\text{m}$  and geometric standard deviation of 0.2.

precipitation process that in 30 min converted 94% of the condensate to precipitation.

The size distributions at intermediate times are quite different for this case. Here, the concentration of drizzle drops that formed after about 20 min was much higher than in either the control or the standard seeded cases, and the drizzle concentration remained high throughout the time of precipitation development. Coalescence among the cloud droplets continued to provide a source of drizzle-size drops, and they grew to become the raindrops.

#### f. Discussion

These results were constructed to exaggerate any seeding effects. The case is unrealistic because it would not persist as specified for 30 min and if it did other mechanisms for broadening the droplet spectrum would surely act. The purpose in these calculations is to illustrate that hygroscopic material from flares might have a beneficial effect on precipitation development, through either of two distinct mechanisms: (a) introduction of embryos on which raindrops form, as in conventional hygroscopic seeding; or (b) broadening of the initial droplet size distribution resulting in acceleration of all stages of the coalescence process. It appears that the smallest particles in the smoke from the flares, having sizes around  $0.3 \mu\text{m}$ , are not beneficial even though they are larger than most natural CCN. The most important contribution to the seeding effect in these calculations arises from the particles in the size range from 1 to  $10 \mu\text{m}$ , and a seeding flare that produced a size

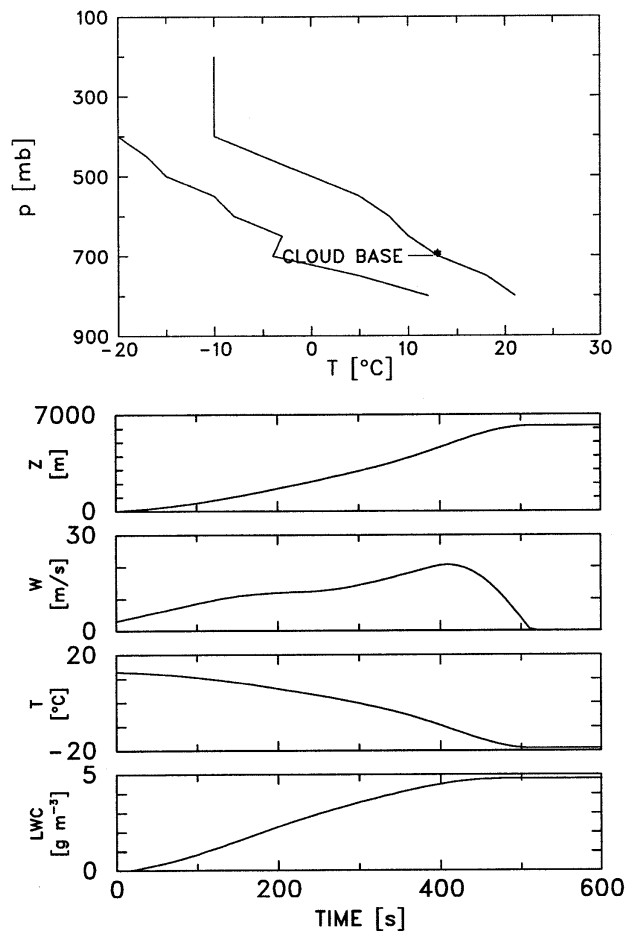


FIG. 6. Temperature and dewpoint sounding (top) vs pressure, and the history of the liquid water content (LWC,  $\text{g m}^{-3}$ ), temperature ( $T$ ,  $^{\circ}\text{C}$ ), updraft ( $W$ ,  $\text{m s}^{-1}$ ), and altitude above cloud base  $Z$  (m) for a parcel rising in this sounding.

distribution concentrated at these sizes might be more effective than the distribution of Fig. 1.

## 5. Seeding effects calculated for realistic soundings

### a. Continental case

The results in this section are based on realistic soundings and CCN distributions from different areas. The cases represent many areas of the world where cloud seeding might be considered. In each case, calculations compare how coalescence would occur in an unmixed parcel for a control case with a natural CCN population and for a seeded case where additional CCN are introduced.

The first case is a continental cloud, with characteristics selected to match the clouds of the interior of South Africa where trials of this seeding strategy are underway. The CCN spectrum was assumed to be the natural spectrum shown in Fig. 3. The sounding, shown in Fig. 6, was selected because rain showers and vig-

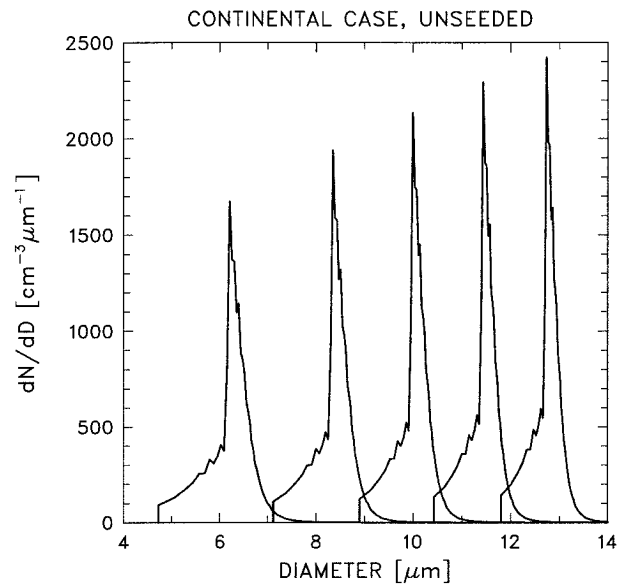


FIG. 7. Droplet size distributions  $dN/dD$  as functions of droplet diameter  $D$  for 20-s intervals beginning 20 s after passage through cloud base. The droplet concentration near cloud base was  $990 \text{ cm}^{-3}$ . The altitude of the parcel 100 s after passage through cloud base was 575 m above cloud base, where the liquid water content was  $0.97 \text{ g m}^{-3}$ .

orous updrafts were present on that date. The cloud base was at 700 mb, where the temperature was  $+13^{\circ}\text{C}$ . The cloud base updraft was taken to be  $3 \text{ m s}^{-1}$ , approximately as observed. The resulting updraft profile is also shown in Fig. 6. To avoid the complications associated with calculating evaporation in downdrafts, the parcel was held at its maximum altitude once the calculated updraft became negative, about 8 min after the parcel passed through cloud base.

Figure 7 shows the early activation of the CCN spectrum and the development of the droplet size distribution near cloud base for the control case. These results are as expected and conform to characteristics found in many other calculations, such as those of Lee and Pruppacher (1977) or Fitzgerald (1974). After 100 s and ascent to 575 m above cloud base, the mean diameter was  $12.7 \mu\text{m}$  and the standard deviation was  $0.37 \mu\text{m}$ , giving an exceptionally small coefficient of variation (or dispersion) of 0.03. The bin resolution for the main peak was about  $0.02 \mu\text{m}$  at this time, so the early shape of the droplet spectrum was represented very accurately. (A later section will consider the case of an artificially broadened spectrum that may be more realistic.)

Figure 8 shows the subsequent development of this droplet spectrum through the combined effects of condensation and coalescence, for the control and the seeded cases. In the control case, represented by thin lines in the figure, precipitation developed slowly, so that raindrops with diameters above  $0.5 \text{ mm}$  just appear in this plot after 10 min. Elimination of the particles larger than  $1 \mu\text{m}$  from the CCN spectrum led to *more* precip-

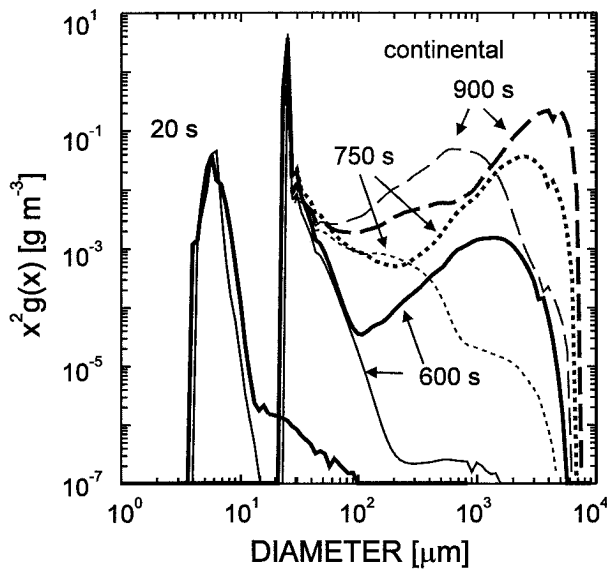


FIG. 8. Mass distribution functions, as in Fig. 4, showing the results of condensation and coalescence for the continental case, after 20, 600, 750, and 900 s of calculation. The solid lines denote results for 20 s and 600 s, the short-dashed lines denote results for 750 s, and the long-dashed lines denote results for 900 s; thin lines are the results for the control case, and thick lines are for the seeded case.

itation after 900 s, so the rain was not produced exclusively from the largest CCN. Instead, the rain mostly formed from coalescence among the largest drops in the main peak of the droplet size distribution. The two sources of precipitation in the control case are reflected in the two-bulge shape of the size distribution at 750 s. (When CCN larger than  $1.0 \mu\text{m}$  were excluded, the bulge at millimeter diameters was absent.) The raindrop concentration that formed after 900 s was  $2.7 \text{ L}^{-1}$ , a concentration shown in Fig. 3a to correspond to the CCN concentration larger than  $1\text{--}2 \mu\text{m}$ . Therefore, CCN having sizes at least this small must have been responsible for the precipitation formation because there was no significant breakup in the calculations.

Only about 12% of the condensate was converted to rain in 15 min, although at that time the precipitation process had been initiated and was accelerating rapidly. In contrast, after 15 min 53% of the condensate was in precipitation in the seeded case. Seeded precipitation formation occurred in a manner similar to that in the control case, but both modes (the growth of the large-droplet portion and the production of the drizzle by coalescence among the cloud droplets) proceeded faster.

Figure 9 shows similar results for seeding with  $150 \text{ cm}^{-3}$  KCl particles having a lognormal size distribution with a geometric mean diameter of  $1.0 \mu\text{m}$  and a geometric standard deviation of 0.2. The development was quite different in this case. The initial size distribution was bimodal and very broad, had a lower total concentration ( $897$  vs  $990 \text{ cm}^{-3}$ ), and included much larger droplets than in the control case. The calculated dispersion after 100 s was 0.22 in this case, in contrast to

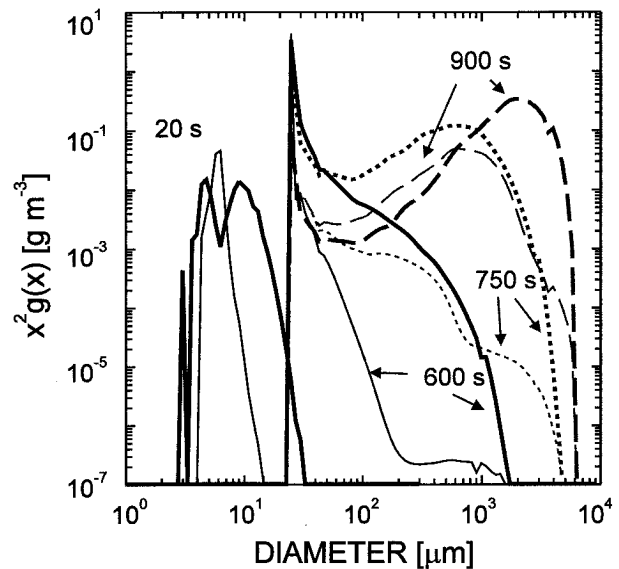


FIG. 9. Mass distribution functions, as in Fig. 8, showing (as thick lines) the results of condensation and coalescence for the continental case when seeded with  $1\text{-}\mu\text{m}$  particles (in a distribution as described in the text), with the control results (thin lines) for reference.

0.07 in the control case. The precipitation formation proceeded through the production of very high concentrations of drizzle drops (with diameters larger than  $100 \mu\text{m}$ ); after 10 min, there were  $31 \text{ L}^{-1}$  such droplets, while there were only  $0.03 \text{ L}^{-1}$  in the control case. After 15 min, this calculation transferred 95% of the condensate to precipitation, so these results indicate even more precipitation formation than in Fig. 8.

#### b. Maritime case

Corresponding results for a maritime case are shown in Fig. 10. The sounding for this case was selected from observations at Hilo, Hawaii, and a CCN spectrum with  $C_1 = 50 \text{ cm}^{-3}$  and  $k = 0.7$  was used in accord with some measurements there (Hudson 1993; J. Hudson 1991, personal communication). The temperature and pressure at cloud base were taken to be  $20^\circ\text{C}$  and 950 mb, common conditions observed near Hilo. The parcel that rose in this sounding developed a maximum liquid water content of  $5.5 \text{ g m}^{-3}$  after rising 3.4 km above cloud base. The seeded calculation included an additional  $30 \text{ cm}^{-3}$  KCl particles with the size distribution of Fig. 1 (dashed line).

Calculated droplet concentrations were only about  $67 \text{ cm}^{-3}$ . Droplets grew to drizzle sizes by condensation, so that the coalescence process was initiated early and proceeded rapidly. In the control case, more than 67% of the condensate was converted to precipitation in 700 s, and more than 99% in 900 s.

Rain developed in similar ways in the seeded and control cases, and was affected only slightly by seeding. In the seeded case, a large-droplet component persisted

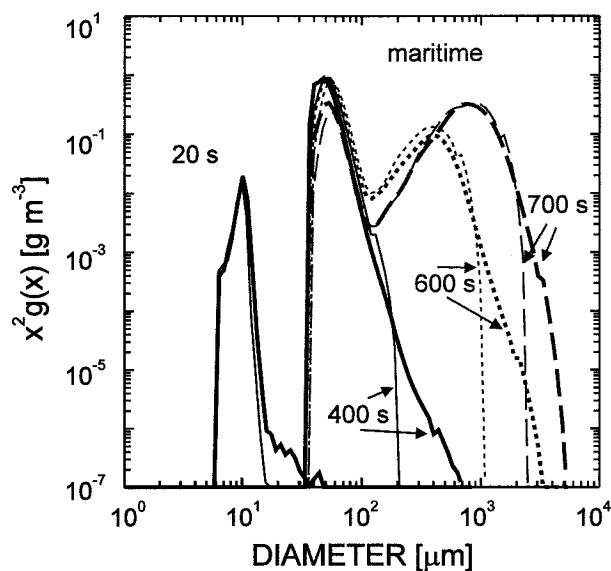


FIG. 10. Mass distribution functions, as in Fig. 8, showing the results of condensation and coalescence for the seeded (thick lines) and control (thin lines) maritime cases, after 20, 400, 600, and 700 s of growth.

throughout the time of the calculation, but seeding also increased the total droplet concentration to  $84 \text{ cm}^{-3}$ . The result was a slight decrease in the net rate of precipitation development. This small decrease was changed to a small increase in precipitation when the calculation was repeated with a size distribution for the seeded material that had a main peak centered at  $0.5 \mu\text{m}$  instead of  $0.3 \mu\text{m}$ .

### c. Intermediate case

Results for an intermediate case are shown in Fig. 11. The sounding was taken from Montana, in the High Plains of the United States, for which the cloud base was at 770 mb and  $13^\circ\text{C}$ . Intermediate CCN concentrations (characterized by  $C_1 = 300 \text{ cm}^{-3}$  and  $k = 0.7$ ) were used and the Junge concentration parameter (cf. section 3b) was changed to  $2 \times 10^{-14}$ . A seeding concentration of  $100 \text{ cm}^{-3}$  was used for this case, with the standard size distribution of Fig. 1 and the adjusted ( $0.5 \mu\text{m}$ ) size distribution used for the maritime case. Figure 11 shows the results for the adjusted case, which gave a small (few percent) acceleration in precipitation formation; the standard CCN distribution gave a small decrease for a seeding concentration of  $100 \text{ cm}^{-3}$  and a small increase for a seeding concentration of  $30 \text{ cm}^{-3}$ . In all cases, effects of seeding were small and the main effect was to produce a small concentration of large drops.

With an initial  $3 \text{ m s}^{-1}$  updraft at cloud base, the droplet concentration that developed was about  $350 \text{ cm}^{-3}$ . After 700 s about 35% of the condensate was in precipitation-size hydrometeors, so the rate of conver-

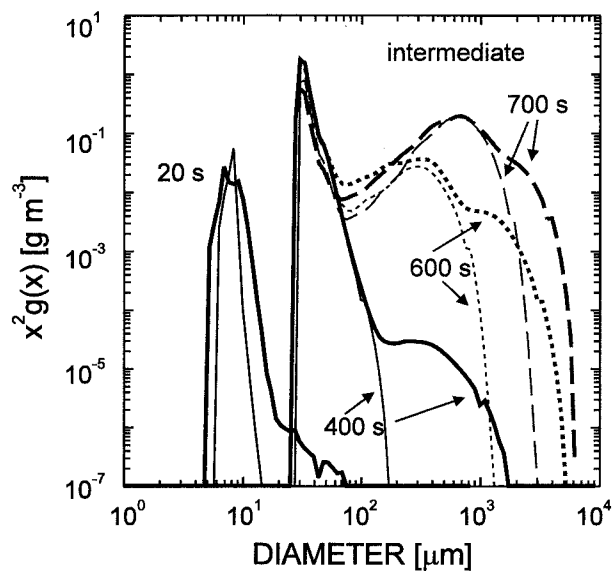


FIG. 11. Mass distribution functions, as in Fig. 10, showing the results of condensation and coalescence for the control and seeded intermediate cases.

sion to precipitation was intermediate between the other two cases as expected. This growth via coalescence in the control case occurred despite the very narrow initial size distribution that developed; after ascent through 1 km the droplet mean diameter was  $22.0 \mu\text{m}$  and the standard deviation was only  $0.30 \mu\text{m}$ .

For seeding with  $100 \text{ cm}^{-3}$  KCl particles for which the smallest lognormal distribution is shifted to have a geometric mean diameter of  $1.0 \mu\text{m}$  and a geometric standard deviation of 0.2, the precipitation developed considerably more rapidly, as shown in Fig. 12. As in the continental case, the initial size distribution was bimodal and significantly broader than in the unseeded case, and drizzle production was enhanced. After 700 s, 75% of the condensate was converted to precipitation, more than double than of either the unseeded case or the case seeded with the standard size distribution.

### d. Summary

The standard size distribution used to represent the flares (Fig. 1) produced marked acceleration of the calculated rates of coalescence in continental clouds with cloud base droplet concentrations of around  $1000 \text{ cm}^{-3}$ , but had small negative effects in the cases selected to represent maritime or intermediate clouds (with cloud base droplet concentrations of about 50 and 300, respectively). Negative effects arose from the small particles in this size distribution, which caused the droplet concentrations in these clouds to increase. However, a small adjustment in the size of the particles, increasing the mean size from about  $0.3$  to  $0.5 \mu\text{m}$ , changed these negative effects to small positive ones and also accelerated the rate of coalescence in continental clouds.

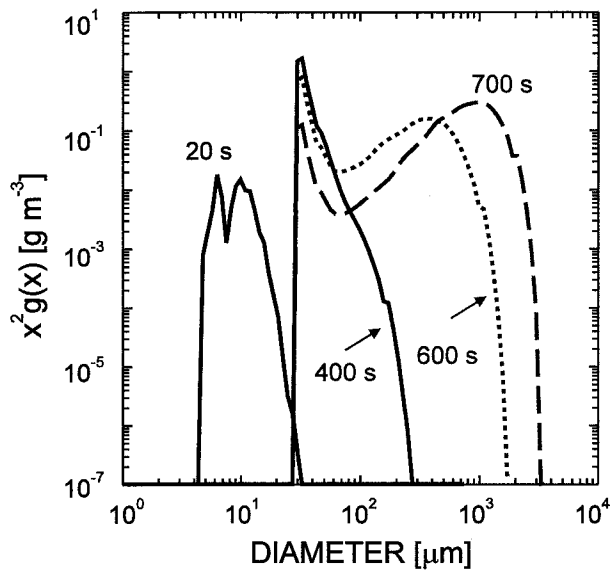


FIG. 12. Mass distribution functions, as in Fig. 10, showing the results of condensation and coalescence for the seeded intermediate case, for seeding with a size distribution having geometric mean diameter of  $1.0 \mu\text{m}$ .

When the calculations were repeated for a size distribution of seeding material having a  $1.0\text{-}\mu\text{m}$  geometric mean size, precipitation developed significantly faster, so that the amount of precipitation at given times was approximately double that for the cases seeded with the standard size distribution.

## 6. Calculations for other size distributions

### a. Broadening of the droplet spectrum

Observed droplet size distributions are almost always significantly broader than those produced by calculations such as the preceding ones. Although there is clear evidence linking broadening of the droplet size distribution to mixing, it may be the case that most of the discrepancy in unmixed regions is the fault of the instruments because the size distributions predicted for unmixed conditions are narrower than the resolution of most droplet spectrometers. However, to study the possible effects of broader droplet spectra on these calculations, some droplet size distributions were broadened artificially during condensational growth. Broadening effects such as those discussed by Srivastava (1989) are examples of effects that could be represented by this forced broadening of the droplet spectrum.

For this broadening, droplets in each bin were reassigned to other bins according to a gamma probability distribution function in mass. To conserve mass, the mean of the distribution was the actual mass corresponding to the bin being redistributed, but the dispersion of the distribution was selected to be 50% of the mean mass in order to provide a dispersion in diameter of about 0.15.

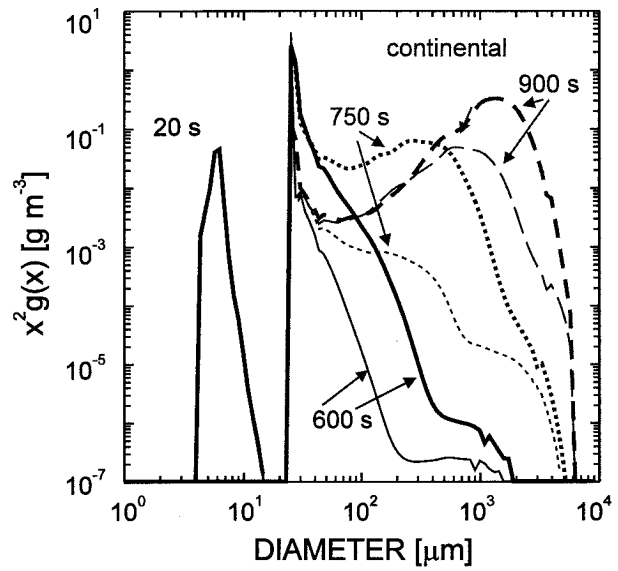


FIG. 13. Mass distribution functions as in Fig. 10, for various times after passage through cloud base, for the continental case after artificially broadening the droplet size distribution as described in the text. For reference, the unbrodden control case is also shown (thin lines).

Figure 13 shows results obtained for the natural continental case, when a single such broadening step was applied 50 mb above cloud base. The droplet size distributions remain narrow, but not so extreme as in the earlier calculations shown in Fig. 8. After 900 s almost all (88%) of the condensate was converted to precipitation versus about 12% without this broadening step. The addition of  $150 \text{ cm}^{-3}$  hygroscopic particles still accelerated the process, but the effect was substantially reduced. If conversion of 10% of the condensate to precipitation is taken as a threshold for the initiation of precipitation, then this threshold was reached in 892 s for the unbrodden control case, 749 s for the unbrodden seeded case, 770 s for the control case after broadening, and 738 s for the seeded case with broadening. The advantage that seeding provides can thus be reduced substantially if there is a source of broadening beyond that incorporated in these calculations.

While entrainment and associated mixing provide a source of such broadening, Rokicki and Young (1978) demonstrated that the accompanying reduction in liquid water content strongly inhibits coalescence growth. This was also evident in the calculations presented in this paper. When the droplet concentration at each step after 300 s was reduced so that the liquid water content in the parcel remained 50% of the value expected for adiabatic ascent, the additional times required for conversion of 50% of the remaining condensate to precipitation approximately doubled, as expected from the nature of the coalescence equations. Even with broadening as forced for Fig. 13, the rate of coalescence was slowed substantially by this reduction in liquid water content

in comparison to the adiabatic but unbroadened case. Any significant reduction in liquid water content associated with entrainment can work against and perhaps offset the broadening effects accompanying such mixing.<sup>2</sup>

In cases where vertical cycling and mixing of parcels occurs, Telford and Chai (1980) argued that the resulting broadening of the droplet size distribution can accelerate the production of rain by creating large drops. That possible source of broadening also is not incorporated in the closed-parcel calculations of this paper, which are intended to apply to the initial development in an unmixed region of cloud. Hygroscopic seeding might have little effect if such cycling determines the rate of production of precipitation embryos, and the calculations of this paper would not apply to that case.

### b. Mixed size distributions

It might be expected that seeding could introduce variability in the CCN population at cloud base, so that mixing of the various spectra that develop in different parts of the cloud base could lead to broadening of the size distribution at higher levels in the cloud. To investigate this possibility, the size distributions developed in natural and seeded cases were mixed together at some level in the ascent, and the calculations were then resumed with the combined size distributions. However, the resulting coalescence rate was always intermediate between the seeded and unseeded cases, and showed no enhancement from this mixing. The apparent reason was that the narrowing effects of condensation compressed the combined spectrum into a narrow peak similar to that in the natural or seeded case, leaving the only significant difference between the two cases at the largest sizes that grow from the seeded CCN. This may pose a problem for seeding strategies based on cloud base release of hygroscopic material, because if the material is diluted substantially before initiation of coalescence can occur then the development of precipitation will also be slowed by that dilution.

## 7. Higher concentrations of giant particles

The calculations presented in section 5 are based on a CCN distribution that does not include realistic contributions from giant and perhaps insoluble natural particles. Johnson (1982) demonstrated that such particles

<sup>2</sup> Entrainment of dry air after activation of the CCN but during ascent of the parcel can accelerate coalescence, however, if it reduces the number concentration of droplets and the remaining droplets then grow more rapidly. In calculations where the droplet concentration was reduced to provide 50% of the liquid water content for adiabatic ascent at each step after 100 s, instead of after 300 s, the rate of conversion to precipitation was even faster than in the reference case without dilution because the diluted droplets then grew faster by condensation than in the undiluted case.

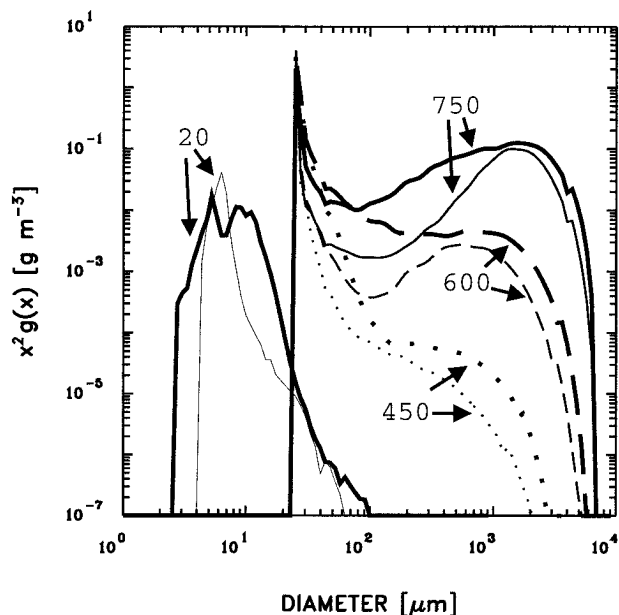


FIG. 14. Mass distribution functions, as in Fig. 8, showing the results of condensation and coalescence for seeded (thick lines) and control (thin lines) cases, for an initial aerosol size distribution with enhanced concentrations of giant particles. Results are shown after 20, 450, 600, and 750 s of growth.

can play a significant role in the initiation of precipitation, so calculations similar to those of section 5 were repeated with much higher concentrations of natural giant particles. Specifically, the parameter  $A$  (cf. section 3b) was increased from  $10^{-13}$  to  $10^{-12}$ , and the diameters to which the size distribution given by (2) applied were from 0.1 to 10  $\mu\text{m}$ , with the concentrations at larger sizes selected as before to give a continuous match to this intermediate size range. This distribution is approximately consistent with that used by Johnson (1982) or presented by Hobbs et al. (1985a), except that it was assumed that the particles were entirely soluble. This case thus probably represents a considerable overestimate of the true effect of the particles with diameters exceeding 1  $\mu\text{m}$ .

The results are shown in Fig. 14. As in Johnson's (1982) results, the development of precipitation was considerably more rapid when these giant natural particles were included. However, seeding still accelerated precipitation formation significantly. For the case shown, with seeding particles of 1- $\mu\text{m}$  geometric mean diameter (as in Fig. 5), the effect of seeding was quite substantial. For example, the amount of precipitation converted to precipitation in 750 s increased from 31% to 50% as a result of seeding. The precipitation still developed quite differently in the seeded and unseeded cases, with the seeded case developing much more drizzle early in the evolution to precipitation. The effect of seeding was less pronounced, but still positive, for the standard size distribution of seeding material shown in Fig. 1.

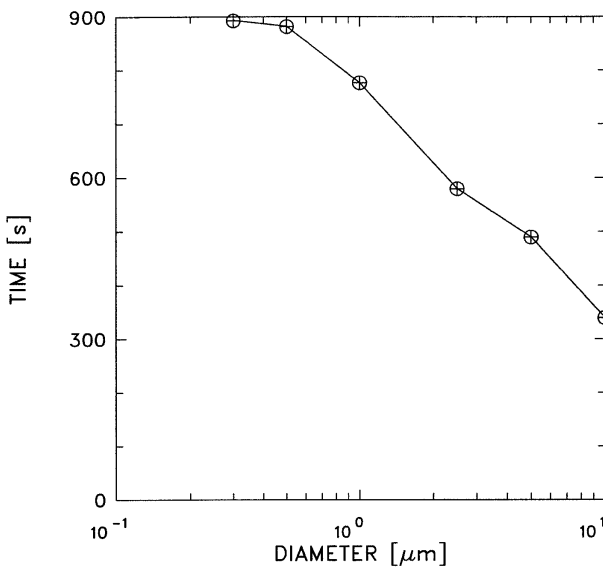


FIG. 15. Time required for conversion of 50% of the condensation to precipitation, for the standard continental case used in this paper, as a function of the assumed geometric mean size of the seeding particles. All calculations used  $150 \text{ cm}^{-3}$  as the concentration, and 0.2 for the geometric mean standard deviation of the size distribution (assumed to be lognormal).

## 8. Optimization of the seeding strategy

### a. Varying the concentration

When the calculations for seeded clouds were repeated with different concentrations of seeding material, it was found that for the continental case used in this paper the conversion to precipitation (measured by the liquid water content present in drops larger than 0.5-mm diameter) was fastest for concentrations of the seeding material from 50 to  $200 \text{ cm}^{-3}$ . If the concentration was increased to more than  $500 \text{ cm}^{-3}$ , the conversion rate was slower than in the natural cloud, and, for concentrations smaller than about  $10 \text{ cm}^{-3}$ , precipitation formation was not significantly faster than in the natural case. Other conditions might favor other seeding rates, but for this case it appears that the optimum seeding concentration is also one that can easily be produced by appropriate dilution of the smoke from the airborne flares.

### b. Varying the mean size

Increasing the mean size of the seeding material in the calculations increased its effectiveness markedly. The times required for conversion of 50% of the condensate to precipitation, for a series of calculations in which the geometric mean radius of the hygroscopic particles was varied, are shown in Fig. 15. The rate of conversion to precipitation continued to increase for sizes up to  $10\text{-}\mu\text{m}$  geometric mean diameter, and the growth rates in these cases were much faster than for small hygroscopic particles. This may be an unrealistic

seeding strategy because of the large mass of salt required, but these results suggest that increasing the size of the particles above those used in the present trials may be beneficial.

Interestingly, the cloud base droplet concentration steadily *decreased* as the seeding concentration increased from more than  $1000 \text{ cm}^{-3}$  for sizes smaller than  $0.5 \mu\text{m}$  to less than 150 for cases with sizes larger than  $5.0 \mu\text{m}$ . In the  $5.0\text{-}\mu\text{m}$  case, no natural CCN were activated near cloud base, but the resulting concentration of droplets was so low that 50 mb above cloud base a second activation region was present and additional small droplets were produced from the natural CCN. The newly activated droplets were depleted by the growing precipitation droplets, and there was continued activation and depletion of new droplets during the ascent of the parcel.

### c. Comparison to seeding with giant particles

Although positive effects resulted from using hygroscopic particles of about  $0.5\text{-}\mu\text{m}$  diameter, these calculations developed precipitation much faster as the size of the particles was increased. To compare these results with those expected from seeding with giant hygroscopic particles (typically having diameters of about  $10 \mu\text{m}$  but concentrations representative of precipitation embryos), calculations were also performed with low concentrations of such particles. These calculations led to significantly increased conversion rates in comparison to the rates expected with smaller particles. In one example, for the same conditions under which the time for conversion of 50% of the condensate to precipitation was changed from 865 s (natural case) to 700 s (seeded case), seeding with  $10\text{-}\mu\text{m}$  giant hygroscopic particles reduced the time required to 570 s for a seeding concentration of  $10 \text{ L}^{-1}$ .

Although the conversion to precipitation was much faster in the calculations with  $10\text{-}\mu\text{m}$  particles, the nature of the growth to precipitation differed from that calculated for  $1.0\text{-}\mu\text{m}$  hygroscopic particles. The initial giant particles provided embryos that grew to raindrops, as expected, but without the high concentration of drizzle drops that was produced in the cases seeded with higher concentrations of smaller hygroscopic particles. Indeed, seeding with giant particles tended to suppress the formation of drizzle by coalescence because the larger droplets were scavenged by the growing raindrops before they reached drizzle sizes. A representative size distribution showing the evolution to precipitation in a case with  $10\text{-}\mu\text{m}$  embryos is shown in Fig. 16. The initial bimodal spectrum shows the low concentration of large droplets that results from this seeding, and that second peak remains distinct from the small-droplet peak as the precipitation evolves. The result is almost no drizzle production, and only the appearance of raindrops that deplete the cloud water. If the drizzle that is produced plays an important role in propagating the

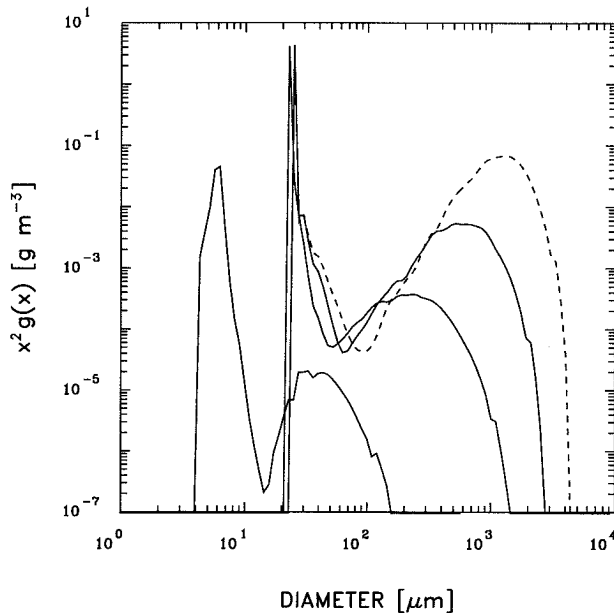


FIG. 16. Mass distribution function like that in Fig. 10 for the standard "continental" case seeded with  $10\text{-}\mu\text{m}$  hygroscopic particles in a concentration of  $10\text{ L}^{-1}$ . The figure shows the contributions to the liquid water content from hydrometeors of different sizes, at times of 20, 400, 500, and 600 s (dotted line) after passage through cloud base.

effect through the cells or among cells of a multicellular storm, there may be an advantage to using smaller hygroscopic particles in an attempt to increase drizzle production throughout the cloud.

## 9. Conclusions and further discussion

It is well established that higher initial droplet concentrations tend to inhibit coalescence, and also that some very large CCN can be beneficial. The calculations presented here suggest that the concentration of accumulation-mode particles may also influence coalescence rates because those particles can increase the sizes of the largest drops in the initial size distribution. Concentrations of such particles comparable to those found beneficial for seeding in these studies are commonly found in polluted industrial air masses, and high concentrations of coarse-mode particles are characteristic of desert dust such as is produced copiously from north-central Africa. Changes in the concentrations of these particles can be expected to influence coalescence rates and precipitation efficiency.

The calculated effects of seeding with hygroscopic flares suggest that the formation of precipitation via coalescence might be accelerated by such seeding, so these results support further investigation of this seeding technique. However, the results presented here should be interpreted with considerable caution because they oversimplify the real process of precipitation formation. They do not incorporate mechanisms that broaden cloud

droplet size distributions (including mixing, stochastic effects during condensation, variable growth trajectories, possible vertical cycling, etc.) They also do not account for sedimentation in a realistic way, and they neglect ice-phase precipitation formation. In most of the clouds to which this seeding technique might be applied, ice-phase precipitation processes are important and often dominant, so a convincing argument regarding enhancement of precipitation by this technique would need to consider those ice-phase processes. Many results of an accelerated coalescence process favor ice-phase precipitation as well; for example, larger droplets accrete on graupel with higher collection efficiencies, and the freezing of drops may accelerate their growth (Johnson 1987). However, negative effects are also possible, for example, from an enhanced secondary ice production process that might produce inefficient glaciation of the clouds. These interactions between an accelerated coalescence process and an ice-phase precipitation process need further investigation.

While we interpret these calculations as supporting the potential value of this approach to cloud seeding, some additional critical problems remain. Among these is a fundamental impediment: Diffusion of material released from aircraft is so slow that it is difficult to influence significant portions of a cumulus cloud by cloud base seeding. The results of Weil et al. (1993) show that only after more than about 10 min can a plume released in a cloud spread over distances of several kilometers, as required to fill an updraft region of even one cell. A possible solution to this problem may lie in seeding the strongest updrafts, which are expected to rise to near cloud top, where any drizzle-size drops produced might spread and be carried downward in the descending flow near cloud edge. In the conceptual model of Blyth et al. (1988), such material would be spread throughout the cloud and might affect large regions of this turret or perhaps other turrets. Such a circulation is supported by the observations of Stith et al. (1990).

The calculations in this paper suggest that the seeding flares might be more effective if the size distribution were shifted toward larger sizes. The particles having diameters near  $0.3\text{ }\mu\text{m}$  apparently did not have beneficial effects and, in some cases, inhibited precipitation formation. However, increasing the mean size to about  $0.5\text{ }\mu\text{m}$  led to positive effects in all cases, and a mean size of  $1.0\text{ }\mu\text{m}$  was very effective while increasing the production of drizzle dramatically. This change to the flares might be particularly beneficial if the mechanism for propagation of the effect through a storm is via the production of drizzle, as speculated in the preceding paragraph.

Suitable clouds for treatment by hygroscopic flares are probably those in which a coalescence process is marginally active but not efficient. Likely candidates include the midwestern United States (with clouds described by Cys 1991), Texas (Rosenfeld and Woodley 1989), Arizona (Battan 1963), Oklahoma (Heymsfield

and Hjelmfelt 1984), South Africa (Krauss et al. 1987), the northern High Plains (Hobbs et al. 1980; Cooper and Lawson 1984), and probably many other similar areas throughout the world. A seeding strategy based on hygroscopic seeding might have wide applicability for the enhancement of summertime rainfall, if the effect of such seeding is to enhance coalescence rates.

Hobbs et al. (1970) and Hindman et al. (1977) noted that large increases in precipitation occurred downwind of some industrial sites known to be good sources of CCN, and they also suggested that the effect may be attributable to the most efficient and largest CCN. Effects of increased CCN concentrations on cloud properties have received considerable attention recently, but little attention has been paid to the factors determining the size distribution of CCN and the potential influences of the largest CCN. Considerations such as those outlined in this paper bear not only on the potential for cloud seeding but also on possible effects of anthropogenic sources of large particles and effects of desert dust and other natural sources on the global precipitation cycle.

*Note in press.* WAC and RTB deeply regret that our coauthor, colleague, and friend Graeme K. Mather died on 15 August 1997. His enthusiasm for the research reported in this and the preceding paper attracted us both to this work, but the development of this seeding technique resulted almost completely from his personal persistence and conviction. He approached field experiments, piloting, cloud seeding, data analysis, and friendships all with the same irresistible enthusiasm. It will be fitting if these papers help stimulate a new approach to weather modification, but in any case the "quest" for a way to enhance precipitation has lost a dedicated champion.

*Acknowledgments.* The experimental work is supported by the Water Research Commission of South Africa. The research manager for this project, George Green, has served an essential role by maintaining its continuity and providing important leadership in management of this project.

#### APPENDIX A

##### List of Symbols

$\alpha$	accommodation coefficient (cf. Fukuta and Walter 1970)
$\beta$	condensation coefficient (cf. Fukuta and Walter 1970)
$\Theta_q$	wet-equivalent potential temperature at cloud base
$\chi$	liquid water content
$\lambda$	thermal conductivity of air
$\lambda^*$	modified conductivity [see Eq. (B3)]
$\rho_s$	density of solution droplet

$\sigma$	surface free energy of solution droplet
$C$	specific heat modified for total water content (cf. Paluch 1979)
$C$	growth factor for condensation [see Eq. (B2)]
$C_1$	number of CCN active at 1% supersaturation
$D$	diffusivity of water vapor in air
$D^*$	modified diffusivity [see Eq. (B4)]
$e$	water vapor pressure
$e_s(T)$	saturation water vapor pressure at temperature $T$
$F(r_a)$	cumulative size distribution of CCN
$i$	van't Hoff factor for solute in solution
$k$	slope of cumulative distribution of CCN concentration [see Eq. (1)]
$k(r_j, r_m)$	collection kernel for collisions between droplets having radii of $r_j$ and $r_m$
$L_v$	latent heat of vaporization of water
$m_s$	mass of solute in CCN on which drop forms
$m_w$	mass of water in droplet
$M_a$	molecular weight of "air" (28.9644 g mole <sup>-1</sup> )
$M_s$	molecular weight of solute
$M_w$	molecular weight of water
$n(n_j)$	drop concentration (of droplets in bin $j$ )
$p$	pressure
$r(r_j)$	drop radius (of droplets in bin $j$ )
$r_a$	radius of CCN
$r_t$	total water mixing ratio
$r_v$	water vapor mixing ratio
$R$	universal gas constant
$S(t)$	saturation ratio $e/e_s(T)$
$S'(t)$	modified saturation ratio [cf. Eq. (B7)]
$t$	time
$T$	air temperature
$x(x_j)$	drop mass (of droplets in bin $j$ )

#### APPENDIX B

##### Details of the Numerical Procedures

###### a. Condensation

For condensation, the Fukuta–Walter equation was used, in the form

$$\frac{dr^2(t)}{dt} = 2[S(t) - 1]C(r, m_s, \alpha, \beta, p, T), \quad (\text{B1})$$

where  $C$  is given by

$$C^{-1} = \rho_s \left[ \frac{RT}{M_w D^* e_s(T)} + \frac{L_v^2 M_w}{\lambda^* RT^2} \right]. \quad (\text{B2})$$

The diffusivity and conductivity in this equation have been modified to account for the effects of the condensation and accommodation coefficient, in the manner of Fukuta and Walter (1970).

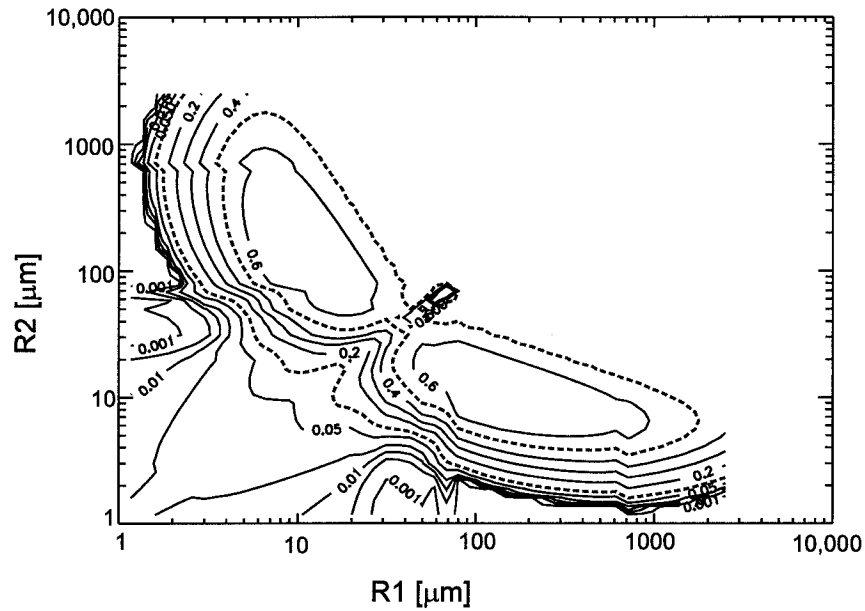


FIG. B1. Collection efficiency (equal to the product of the collision and coalescence efficiency) used for the calculations of this paper, as functions of the two radii  $R1$  and  $R2$  of the colliding drops. Contours correspond to 0.001, 0.005, 0.01, 0.02, 0.05, 0.1, 0.2, 0.3, 0.4, 0.5, 0.6, 0.8, and 1.0, with the 0.1 and 0.5 contours shown as heavy dotted lines.

$$\lambda^* = \lambda \left( \frac{r}{r + \ell_\alpha} \right) \quad (\text{B3})$$

$$D^* = D \left( \frac{r}{r + \ell_\beta} \right), \quad (\text{B4})$$

where

$$\ell_\alpha = \frac{\lambda (2\pi M_\alpha RT)^{1/2}}{\alpha Rp} \quad (\text{B5})$$

$$\ell_\beta = \frac{D}{\beta} \left( \frac{2\pi M_w}{RT} \right)^{1/2}. \quad (\text{B6})$$

The modified saturation ratio  $S'$ , which accounts for the effects of droplet curvature and dissolved solute, is

$$S' = S \left( 1 + \frac{im_s M_w}{m_w M_s} \right) e^{-2\sigma M_w / \rho_s r RT} - 1. \quad (\text{B7})$$

The solution density  $\rho_s$ , surface free energy  $\sigma$ , and van't Hoff factor  $i$  all are functions of the concentration of solute in the drops, and appropriate functional relationships were used [from the CRC tables of Weast (1966) for  $\rho_s$  and  $\sigma$ , and from Low (1969) for  $i$ ]. However, the effect of the derivative of the van't Hoff factor with molality, discussed by Young and Warren (1992) and Young (1993), was not included in these calculations. The pressure and temperature dependence of the diffusivity, conductivity, and latent heat were also represented in the calculations. The Goff-Gratch formula

(cf., e.g., List 1968) was used for the saturation water vapor pressure  $e_s(T)$ .

#### b. Coalescence

Figure B1 shows the collection efficiency assumed in these calculations. Because the algorithm used to represent coalescence kept track of the concentration of drops in each bin and calculated collision rates among those drops, no Jacobian was needed to represent the collection kernel. The algorithm represented the cumulative effects of coalescence in terms of  $dn_j/dt$  and  $d(n_j x_j)/dt$ , where  $n_j$  is the concentration and  $x_j$  is the droplet mass of the bin with index  $j$ , as follows.

For each bin  $j$

for each bin  $m$  representing a smaller drop

$$x = x_m + x_j = \text{mass of new drop}$$

$$g = n_j n_m k(r_j, r_m)$$

$i$  = index of bin nearest to  $x$

add  $g$  to  $(dn_i/dt)$ ,

subtract  $g$  from  $(dn_j/dt)$  and  $(dn_m/dt)$

add  $gx$  to  $[d(n_i x_i)/dt]$ ,

subtract  $gx_j$  from  $[d(n_j x_j)/dt]$

subtract  $gx_m$  from  $[d(n_m x_m)/dt]$ .

The collection efficiency was the product of the collision efficiency (Klett and Davis 1973; Beard and Grover 1974) and the coalescence efficiency of Beard and Ochs (1984). The analytical representation of the latter, extended to all sizes, was used with the efficiency limited to the range 50%–100% as they recommended. The kernel  $k(r_j, r_m)$  was obtained by calculating the difference in fall speed for each pair of drops, multiplying by the area of a circle with radius equal to the sum of the drop radii, and then multiplying by the collection efficiency obtained by interpolation in a  $50 \times 50$  tabulation of the logarithms of the collection efficiency. The tabulation spanned radii from 1 to 2500  $\mu\text{m}$  (tabulated in logarithmic intervals) as shown in Fig. B1. For smaller radii the efficiency was assumed to be zero and for larger radii the efficiency was held constant at the 2500- $\mu\text{m}$  value. The terminal fall speeds were represented, with full pressure and temperature dependence, using the procedure of Beard (1976).

When the collision efficiencies of Davis (1984) and Rogers and Davis (1990) were used in place of the Klett and Davis (1973) values, the resulting growth rates were slowed slightly from those presented in this paper. However, the patterns and relative effects of seeding presented in this paper were still present in those results, and there was no change to the qualitative conclusions of this paper.

### c. The integration technique

Once derivatives were calculated for condensation and coalescence, the following integration procedure was used. First, the contributions to the derivatives  $dm/dt$  from condensation and from coalescence were added for all activated droplets. Then an adaptive-step version of a Runge–Kutta scheme was used for the growth of each droplet. To select the step size, Runge–Kutta steps were evaluated to the fifth order and to the fourth order, and the difference used to estimate the error in the fourth-order step. If this exceeded a selected tolerance (typically  $10^{-7}$  g  $\text{m}^{-3}$ ), then the step size was reduced and the step was repeated until the tolerance was met; if the error estimate was smaller than the tolerance, then the next trial step was increased. This concentrated the steps in regions that most affected the transfer of liquid water content from cloud droplets to precipitation. The method was essentially that of Cash and Karp (1990) as described in Press et al. (1992; cf. p. 716), except that absolute rather than relative error limits were used. In addition, the step size was kept smaller than 10% of the time constant for relaxation of the supersaturation, to avoid instability in prediction of the supersaturation (which was kept as a prognostic variable throughout the calculations to treat cases of renewed droplet activation during acceleration of parcels or during depletion of cloud droplets by precipitation). This scheme resulted in the use of small time steps (typically 0.02–0.1 s) in the initial stages of the calculation, but time steps of 1–

10 s for steady updraft conditions late in the calculations.

If the concentration of drops in a given category ever became negative at the end of a time step, the time step was reduced and the step repeated until the result was positive. Negative concentrations arose only when decay rates were used for too long a time step; collision rates are proportional to the concentration of droplets and thus must decay exponentially to zero.

Other integration methods including Euler, fixed-step Runge–Kutta, and a predictor–corrector scheme were used for test integrations and compared to the results obtained by the selected method. Consistent results were obtained using all these methods, but the selected method provided the best compromise between speed and accuracy.

Using this approach, both condensation and coalescence contributed to the rate of change of the mass of the droplets in a given bin. However, the number concentrations were affected only by coalescence, breakup, and dilution by expansion. The mass increment calculated in this way was divided among all drops in the bin (after the number was adjusted as calculated in the preceding section). Following this step, the rate of change of the water vapor pressure was calculated by considering the rate of ascent of the parcel and the rate of condensation, and this rate of change was applied to the vapor pressure in a simple Euler step. The vertical wind was adjusted by application of the buoyancy obtained by reference to the environmental sounding, and the altitude step and pressure step were calculated. The temperature was then calculated as described in section 3b, and pressure and temperature time derivatives were saved for the next dilution of the drop concentration.

After the growth calculation, a new vapor pressure was calculated by depleting the vapor pressure to account for condensation, then diluting the result to account for expansion to the next level. The equation used was

$$\frac{de}{dt} = -\frac{RT}{M_w + r_t M_d} \frac{d\chi}{dt} + \frac{e}{p} \frac{dp}{dt}, \quad (\text{B8})$$

where  $\chi$  is the liquid water content and  $r_t$  is the (constant) total water mixing ratio, determined at cloud base.

At this point, the increments in pressure and water vapor pressure were calculated from the vertical wind and the hydrostatic equation and were applied to the air parcel, and the droplet concentrations were diluted in proportion to the change in air density. The new temperature of the air parcel was determined iteratively from the equation

$$T' = \Theta_q \left( \frac{p - e}{p} \right)^{R/C_p} e^{L_v r_v / C_p T}, \quad (\text{B9})$$

where  $\Theta_q$  is the constant wet-equivalent potential temperature calculated at cloud base and saved for this use, and  $T'$  is the revised estimate of the temperature  $T$ .

(Usually, one step was sufficient, but this was iterated until the consecutive changes were smaller than  $10^{-7}T$ .) Then a new virtual temperature was calculated, and buoyancy was determined by comparison to the assumed sounding. In response, the vertical velocity was changed according to the calculated acceleration.

As a check, the total water mixing ratio was calculated and monitored for significant changes. Because the coalescence procedure enforced conservation of water substance, this was only a protection against rounding or other numerical problems in the treatment of the vapor pressure via (B8).

#### APPENDIX C

##### Comparison to Other Coalescence Schemes

###### a. Comparison to analytical solutions

Analytical solutions to the coalescence equation have been obtained by Golovin (1963) and Scott (1968) for special forms of the collision kernel. Figures C1 and C2 show two comparisons to these analytical solutions for different initial distributions. The errors produced by the numerical procedures were in the direction of slightly underestimating growth rates for the largest sizes, in contrast to most other cases in which numerical diffusion produces too fast a growth rate. The results were within a few percent of the analytical solutions for the periods of these calculations, which correspond to about an hour of coalescence growth.

###### b. Comparison to the method of Berry and Rinehardt

The method used here for integration of the coalescence equation has the potential to slow transfer of the

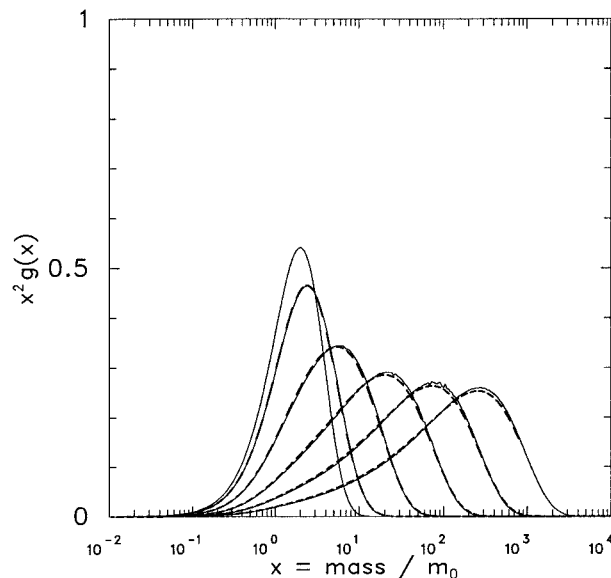


FIG. C1. Evolution of the mass distribution function calculated as in this paper (thin solid line) compared to the analytical solution of Golovin (1963; heavy dashed line) for the same initial distribution.

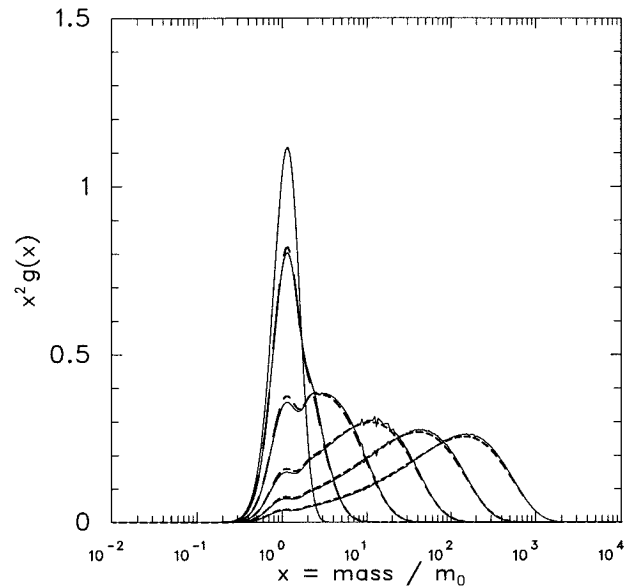


FIG. C2. As for Fig. C1 but for a narrower distribution, as compared to the analytical solution of Scott (1968).

condensate to precipitation because of the bias discussed earlier. To check for the possible significance of this bias and also as a test of the new procedures, integrations using this method were compared to corresponding integrations using the method of Berry and Rinehardt (1974a, b). The specific version used was that described by Hall (1980), using collision efficiencies and initial distributions as specified there. This comparison has value beyond supporting the validity of the present calculations because the bias in the present technique is expected to be toward slowed growth, while the potential bias in the Berry and Rinehardt technique is more likely toward accelerated growth. Thus, the comparison between these two techniques also establishes some expected limits to the accuracy of both.

Both calculations were initialized using the same single gamma distribution described by Berry and Rinehardt (1974b) with a mean radius of  $14 \mu\text{m}$  and a liquid water content of  $1 \text{ g m}^{-3}$ .

Figure C3 shows the results obtained using the method described in this paper and that obtained using the method of Berry and Rinehardt (1974a, b). The difference between the two results is in the direction expected for the above biases, but overall the patterns and rates of growth are quite similar in the two cases. Both convert more than 99% of the condensate to precipitation in 1800 s, and both proceed through similar patterns. Part of the small difference may arise from the small but significant (3%) increase in liquid water content that arose when using the Berry and Rinehardt scheme. This increase was not present in the new scheme in which the procedures enforce exact conservation of water.

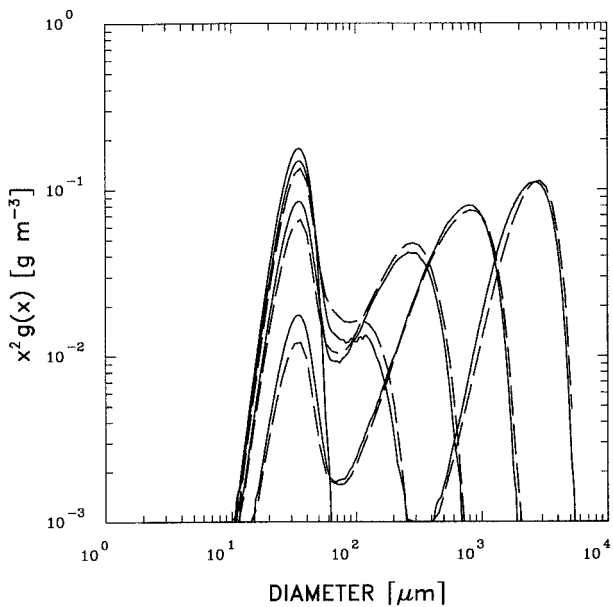


FIG. C3. Mass distribution functions, as in Fig. 4, comparing results obtained using the method described in this paper (solid lines) to those obtained using the method of Berry and Rinehardt (1974a; dashed lines). The initial size spectrum was a gamma distribution function with mean diameter of 28  $\mu\text{m}$ .

### c. Estimates of error limits arising from the integration

One advantage of the Cash–Karp method of integration is that it produces an estimate of the likely error at each time step. These can be accumulated or added in quadrature to obtain a net estimate of the cumulative error arising from the integration. (It would be hoped that the actual error is smaller than this because the integration is actually performed to fifth order, but the error estimate applies to the fourth-order Runge–Kutta formula.)

The selected error limit,  $10^{-7} \text{ g m}^{-3}$  when applied to each step and each bin, normally led to cumulative root-mean-square errors that are the larger of 0.001  $\text{g m}^{-3}$  or 5% of the final value. Furthermore, when the error limit was reduced to  $10^{-8} \text{ g m}^{-3}$ , the result of the integration changed by much less than these estimated errors; the only significant change was that the new error tolerances were much smaller. This indicates that the integration contributes little to the final error.

### REFERENCES

- Alofs, D. J., and T.-H. Liu, 1981: Atmospheric measurements of CCN in the supersaturation range 0.013–0.681%. *J. Atmos. Sci.*, **38**, 2772–2778.
- Barratt, E. W., F. P. Parungo, and R. F. Pueschel, 1979: Cloud modification by urban pollution: A physical demonstration. *Meteor. Res.*, **32**, 136–149.
- Battan, L. J., 1963: Relationship between cloud base and initial radar echo. *J. Appl. Meteor.*, **2**, 333–336.
- Beard, K. V., 1976: Terminal velocity and shape of cloud and precipitation drops aloft. *J. Atmos. Sci.*, **33**, 851–864.
- , and S. N. Grover, 1974: Numerical collision efficiencies for small raindrops colliding with micron size particles. *J. Atmos. Sci.*, **31**, 543–550.
- , and H. T. Ochs III, 1984: Collection and coalescence efficiencies for accretion. *J. Geophys. Res.*, **89**, 7165–7169.
- Berry, E. X., and R. L. Rinehardt, 1974a: An analysis of cloud drop growth by collection: Part I. Double distributions. *J. Atmos. Sci.*, **31**, 1814–1824.
- , and —, 1974b: An analysis of cloud drop growth by collection: Part II. Single initial distributions. *J. Atmos. Sci.*, **31**, 1825–1831.
- Biswas, K. R., and A. S. Dennis, 1971: Formation of a rain shower by salt seeding. *J. Appl. Meteor.*, **10**, 780–784.
- Blyth, A. M., W. A. Cooper, and J. B. Jensen, 1988: A study of the source of entrained air in Montana cumuli. *J. Atmos. Sci.*, **45**, 3944–3964.
- Cash, J. R., and A. H. Karp, 1990: A variable order Runge–Kutta method for initial value problems with rapidly varying right-hand sides. *ACM Trans. Math. Software*, **16**, 201–222.
- Cooper, W. A., 1989: Effects of variable droplet growth histories on droplet size distributions. Part I: Theory. *J. Atmos. Sci.*, **46**, 1301–1311.
- , and R. P. Lawson, 1984: Physical interpretation of results from the HIPLEX-1 experiment. *J. Climate Appl. Meteor.*, **23**, 523–540.
- Czys, R. R., 1991: A preliminary appraisal of the natural structure and seedability of updrafts in Midwestern cumulus at the  $-10^\circ\text{C}$  level. *J. Wea. Modif.*, **23**, 1–16.
- Davis, R. H., 1984: The rate of coagulation of a dilute polydisperse system of sedimenting spheres. *J. Fluid Mech.*, **145**, 179–199.
- Farley, R. D., and C. S. Chen, 1975: A detailed microphysical simulation of hygroscopic seeding on the warm rain process. *J. Appl. Meteor.*, **14**, 718–733.
- Fitzgerald, J. W., 1974: Effect of aerosol composition on cloud droplet size distribution: A numerical study. *J. Atmos. Sci.*, **31**, 1358–1367.
- Fukuta, N., and L. A. Walter, 1970: Kinetics of hydrometeor growth from a vapor-spherical model. *J. Atmos. Sci.*, **27**, 1160–1172.
- Gillespie, D. T., 1975: An exact method for numerically simulating the stochastic coalescence process in a cloud. *J. Atmos. Sci.*, **32**, 1977–1989.
- Golovin, A. M., 1963: The solution of the coagulation equation for cloud droplets in a rising air current. *Bull. Acad. Sci. USSR, Geophys. Ser. (English Transl.)*, **5**, 482–487.
- Hall, W. O., 1980: A detailed microphysical model within a two-dimensional dynamic framework: Model description and preliminary results. *J. Atmos. Sci.*, **37**, 2486–2507.
- Heymsfield, A. J., and M. R. Hjelmfelt, 1984: Processes of hydrometeor development in Oklahoma convective clouds. *J. Atmos. Sci.*, **41**, 2811–2835.
- Hindman, E. E., II, P. V. Hobbs, and L. F. Radke, 1977: Cloud condensation nuclei from a paper mill. Part I: Measured effects on clouds. *J. Appl. Meteor.*, **16**, 745–752.
- Hobbs, P. V., L. F. Radke, and S. E. Shumway, 1970: Cloud condensation nuclei from industrial sources and their apparent influence on precipitation in Washington State. *J. Atmos. Sci.*, **27**, 81–89.
- , M. K. Politovich, and L. F. Radke, 1980: The structures of summer convective clouds in eastern Montana. I: Natural clouds. *J. Appl. Meteor.*, **19**, 645–663.
- , D. A. Bowdle, and L. F. Radke, 1985a: Particles in the lower troposphere over the High Plains of the United States. Part I: Size distributions, elemental compositions and morphologies. *J. Climate Appl. Meteor.*, **24**, 1344–1356.
- , —, and —, 1985b: Particles in the lower troposphere over the High Plains of the United States. Part II: Cloud condensation nuclei. *J. Climate Appl. Meteor.*, **24**, 1358–1369.
- Hudson, J. G., 1993: Cloud condensation nuclei near marine cumulus. *J. Geophys. Res.*, **98**, 2693–2702.
- Johnson, D. B., 1982: The role of giant and ultragiant aerosol particles in warm rain initiation. *J. Atmos. Sci.*, **39**, 448–460.

- , 1987: On the relative efficiency of coalescence and riming. *J. Atmos. Sci.*, **44**, 1671–1680.
- Klazura, G. E., and C. J. Todd, 1978: A model of hygroscopic seeding in cumulus clouds. *J. Appl. Meteor.*, **17**, 1758–1768.
- Klett, J. D., and M. H. Davis, 1973: Theoretical collision efficiencies of cloud droplets at small Reynolds numbers. *J. Atmos. Sci.*, **30**, 107–117.
- Kovetz, A., and B. Olund, 1969: The effect of coalescence and condensation on rain formation in a cloud of finite vertical extent. *J. Atmos. Sci.*, **26**, 1060–1065.
- Krauss, T. W., R. T. Bruintjes, J. Verlinde, and A. Kahn, 1987: Microphysical and radar observations of seeded and unseeded continental cumulus clouds. *J. Climate Appl. Meteor.*, **26**, 585–606.
- Lee, I. Y., and H. R. Pruppacher, 1977: A comparative study of the growth of cloud droplets by condensation using an air parcel model with and without entrainment. *Pure Appl. Geophys.*, **115**, 523–545.
- List, R. J., 1968: *Smithsonian Meteorological Tables*. Smithsonian Institution Press, 350 pp.
- Low, R. D. H., 1969: A generalized equation for the solution effect in droplet growth. *J. Atmos. Sci.*, **26**, 608–611.
- Low, T. B., and R. List, 1982: Collision, coalescence and breakup of raindrops. Part II: Parameterization of fragment size distributions. *J. Atmos. Sci.*, **39**, 1607–1618.
- Mather, G. K., 1991: Coalescence enhancement in large multicell storms caused by emissions from a Kraft paper mill. *J. Appl. Meteor.*, **30**, 1134–1146.
- Ochs, H. T., and K. V. Beard, 1985: Effects of coalescence efficiencies on the formation of precipitation. *J. Atmos. Sci.*, **42**, 1451–1454.
- Paluch, I., 1979: The entrainment mechanism in Colorado cumuli. *J. Atmos. Sci.*, **36**, 2467–2478.
- Press, W. H., S. A. Teukolsky, W. T. Vetterling, and B. P. Flannery, 1992: *Numerical Recipes in C*. 2d ed. Cambridge University Press, 994 pp.
- Rogers, J. R., and R. H. Davis, 1990: The effects of van der Waals attractions on cloud droplet growth by coalescence. *J. Atmos. Sci.*, **47**, 1075–1080.
- Rokicki, M. L., and K. C. Young, 1978: The initiation of precipitation in updrafts. *J. Appl. Meteor.*, **17**, 745–754.
- Rosenfeld, D., and W. L. Woodley, 1989: Effects of cloud seeding in West Texas. *J. Appl. Meteor.*, **28**, 1050–1080.
- Schickedanz, P. T., 1974: Inadvertent rain modification as indicated by surface raincells. *J. Appl. Meteor.*, **13**, 891–900.
- Scott, W. D., 1968: Analytic studies of cloud droplet coalescence. *J. Atmos. Sci.*, **25**, 54–65.
- , and Z. Levin, 1975: A comparison of formulations of stochastic coalescence. *J. Atmos. Sci.*, **32**, 843–847.
- Srivastava, R. C., 1989: Growth of cloud drops by condensation: A criticism of currently accepted theory and a new approach. *J. Atmos. Sci.*, **46**, 869–887.
- Stith, J. L., A. G. Detwiler, R. F. Reinking, and Paul L. Smith, 1990: Investigating transport, mixing and the formation of ice in cumuli with gaseous tracer techniques. *Atmos. Res.*, **25**, 195–216.
- Telford, J. W., and S. K. Chai, 1980: A new aspect of condensation theory. *Pure Appl. Geophys.*, **119**, 720–742.
- Tzivion, S., T. Reisin, and Z. Levin, 1994: Numerical simulation of hygroscopic seeding in a convective cloud. *J. Atmos. Sci.*, **33**, 252–267.
- Weast, R. C., Ed., 1966: *Handbook of chemistry and physics*. The Chemical Rubber Co., Cleveland, Ohio, 1838 pp. [Available from The Chemical Rubber Co., 2310 Superior Avenue, Cleveland, OH 44114.]
- Weil, J. C., R. P. Lawson, and A. R. Rodi, 1993: Relative dispersion of ice crystals in seeded cumuli. *J. Appl. Meteor.*, **32**, 1055–1073.
- Young, K. C., 1993: Effects of simplifications of the Kohler equation on the activation of CCN in an updraft. *J. Atmos. Sci.*, **50**, 2314–2317.
- , and A. J. Warren, 1992: A reexamination of the derivation of the equilibrium supersaturation curve for soluble particles. *J. Atmos. Sci.*, **49**, 1138–1143.